INTERFACE

royalsocietypublishing.org/journal/rsif

Research

Cite this article: Krause AL, Klika V, Woolley TE, Gaffney EA. 2020 From one pattern into another: analysis of Turing patterns in heterogeneous domains via WKBJ. *J. R. Soc. Interface* **17**: 20190621.
http://dx.doi.org/10.1098/rsif.2019.0621

Received: 5 September 2019
Accepted: 9 December 2019

Subject Category:
Life Sciences–Mathematics interface

Subject Areas:
biochemistry, biomathematics, biophysics

Keywords:
Turing instabilities, pattern formation, WKBJ, heterogeneity

Author for correspondence:
Andrew L. Krause
e-mail: krause@maths.ox.ac.uk

†These authors contributed equally to this work.

Electronic supplementary material is available online at https://doi.org/10.6084/m9.figshare.c.4783008.

THE ROYAL SOCIETY PUBLISHING

From one pattern into another: analysis of Turing patterns in heterogeneous domains via WKBJ

Andrew L. Krause[1], Václav Klika[2,†], Thomas E. Woolley[3] and Eamonn A. Gaffney[1]

[1]Wolfson Centre for Mathematical Biology, Mathematical Institute, University of Oxford, Andrew Wiles Building, Radcliffe Observatory Quarter, Woodstock Road, Oxford OX2 6GG, UK
[2]Department of Mathematics, FNSPE, Czech Technical University in Prague, Trojanova 13, 120 00 Prague, Czech Republic
[3]Cardiff School of Mathematics, Cardiff University, Senghennydd Road, Cardiff CF24 4AG, UK

ALK, 0000-0001-9638-7278; VK, 0000-0001-6272-8396

Pattern formation from homogeneity is well studied, but less is known concerning symmetry-breaking instabilities in heterogeneous media. It is non-trivial to separate observed spatial patterning due to inherent spatial heterogeneity from emergent patterning due to nonlinear instability. We employ WKBJ asymptotics to investigate Turing instabilities for a spatially heterogeneous reaction–diffusion system, and derive conditions for instability which are local versions of the classical Turing conditions. We find that the structure of unstable modes differs substantially from the typical trigonometric functions seen in the spatially homogeneous setting. Modes of different growth rates are localized to different spatial regions. This localization helps explain common amplitude modulations observed in simulations of Turing systems in heterogeneous settings. We numerically demonstrate this theory, giving an illustrative example of the emergent instabilities and the striking complexity arising from spatially heterogeneous reaction–diffusion systems. Our results give insight both into systems driven by exogenous heterogeneity, as well as successive pattern forming processes, noting that most scenarios in biology do not involve symmetry breaking from homogeneity, but instead consist of sequential evolutions of heterogeneous states. The instability mechanism reported here precisely captures such evolution, and extends Turing's original thesis to a far wider and more realistic class of systems.

1. Introduction

Since Alan Turing's celebrated work on morphogenesis [1], reaction–diffusion systems have been a paradigm of pattern formation throughout chemistry and biology [2–7]. The most striking aspect of this theory is the emergence of heterogeneity from homogeneity. However, even Turing himself recognized this as an idealization when he wrote, 'Most of an organism, most of the time is developing from one pattern into another, rather than from homogeneity into a pattern.' Here, we concern ourselves with this heterogeneous setting, and determine the generalization of the Turing conditions to a reaction–diffusion system with explicit spatial dependence. We derive conditions for the instability of a heterogeneous steady state into a Turing-type pattern, with both the localization and structure of the pattern depending on the heterogeneity. Under a necessary hypothesis of a sufficiently slowly varying heterogeneous base state, our results clearly differentiate between spatial structure due to inherent spatial heterogeneity, and emergent patterns due to Turing-type instabilities. This then elucidates successive pattern formation in distinct stages.

This transition from one pattern into another has been noted as key in reconciling seemingly divergent theories in morphogenesis [6]. Turing's original theory was that his reaction–diffusion mechanism laid down a prepattern of heterogeneous

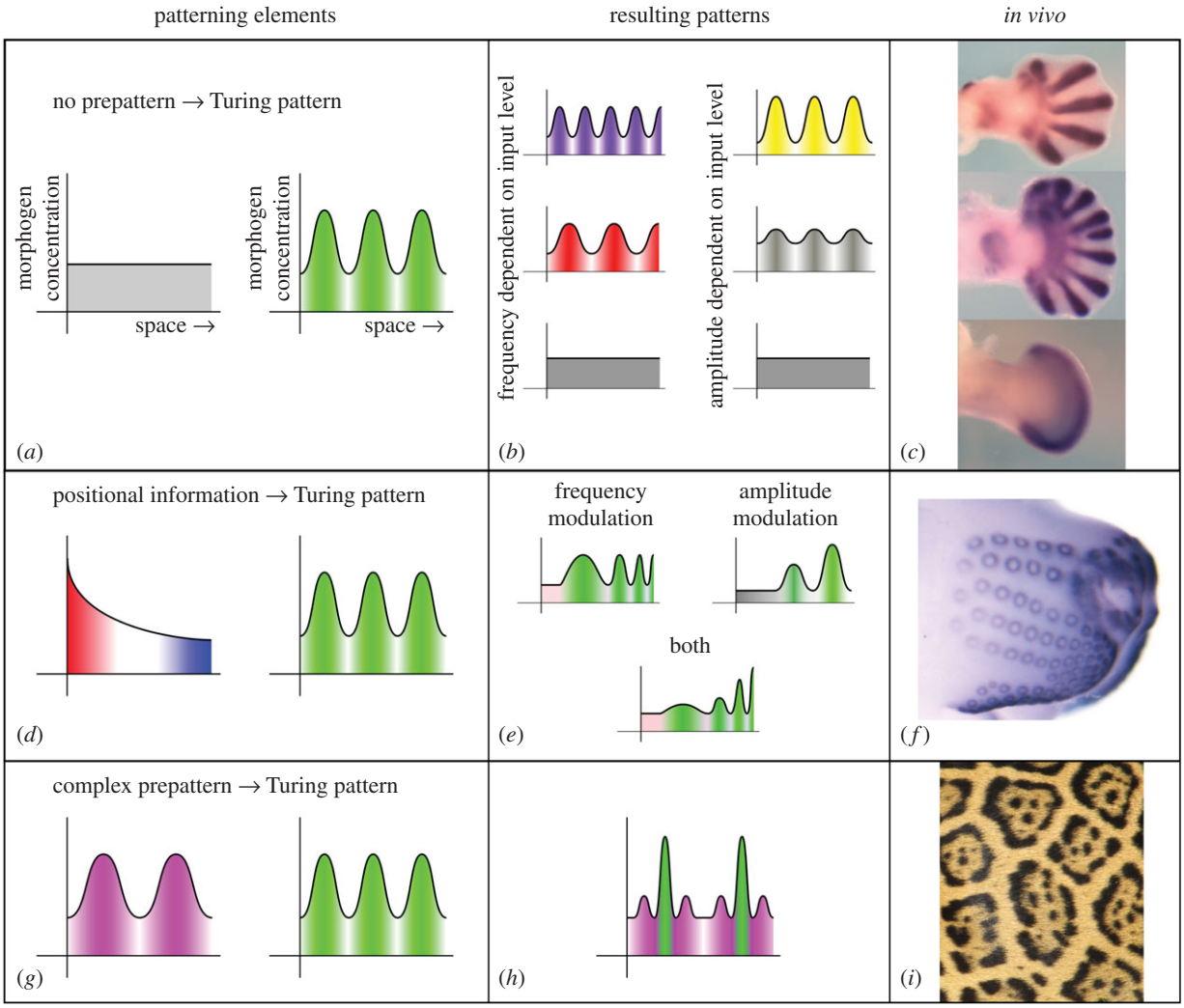

Figure 1. Different interactions of pattern formation mechanisms in development. (*a*) Generic schematic of Turing pattern formation from homogeneity, with different pattern characteristics shown in (*b*), and, in (*c*), a biological example of a developing mouse paw in the presence of altered levels of Hox gene action. Positional information feeding into reaction–diffusion is shown in (*d–e*), consistent with observed structural characteristics of mouse whisker placodes in (*f*). Finally, successive reaction–diffusion patterning is shown in (*g–h*), with the example of Jaguar spots demonstrating large and small-scale pattern formation in (*i*). In particular, the schematic in (*g*) shows a sinusoidal prepattern (left peaks) feeding into a wave mode 3 Turing pattern (right peaks) with, here for illustrative example, the Turing pattern only able to form within the peaks of the prepattern. Thus, each peak forms a disjoint interval. Mouse paw images from Sheth *et al.* [8]. Reprinted with permission from AAAS. Mouse whisker placode image used with permission from Denis Headon. Jaguar picture by Jean Beaufort used under a CC0 Public Domain license from http://bit.ly/JaguarPicture. (Online version in colour.)

morphogen concentration, which then drove cellular differentiation and morphogenesis directly (figure 1*a–c*). This is in contrast to theories of positional information (colloquially 'French-flag' models) whereby cells *a priori* are assigned locations relative to some developmental coordinate system, and perform different functions based on this positional information [9] (figure 1*d*). Spatial heterogeneity provides a way to reconcile these competing theories by allowing positional information to influence reaction–diffusion processes, leading to modulated patterns that are ubiquitous in nature (figure 1*d–f*). Additionally, heterogeneity permits successive reaction–diffusion patterning in stages, whereby patterning at different scales can arise (figure 1*e–g*). This is in line with work implicating chemical and cellular pre-patterns in developmental biology [10–12], such as in the context of organizing different regions along cell boundaries based on sharp variations in gene expression [13,14].

Beyond theories of morphogenesis in developmental biology, models involving reaction–diffusion systems with spatial heterogeneity have been considered in many contexts. Examples include environmental heterogeneity in collective animal dispersal [15–19], reaction–diffusion in domains with non-isotropic growth [20,21], as well as spatial invasion modelling [22,23], and models with differential diffusion leading to spatial inhomogeneity in plant root initiation [24,25]. Spatial heterogeneity has been (numerically) observed to change local instability conditions for pattern formation [26,27], modulate size and wavelength of patterns [28], and localize (or pin) spike patterns in space [29–31]. We also note that the presence of even simple spatial heterogeneity can induce spatio-temporal behaviour, such as changing the stability of patterned states and thereby inducing periodic movement of spike solutions [32,33]. Bifurcation structures of reaction–diffusion equations with spatial heterogeneity have been considered for some time [34]. There is also a large literature on reaction–diffusion systems with strongly localized heterogeneities [35], with [36] recently considering the case of a step-function heterogeneity in the reaction kinetics and deducing local Turing conditions on each side of the step. While we will also deduce local

Turing conditions, we note that this limit is different from the case of smooth spatial heterogeneity we will consider here.

Many experimental applications of reaction–diffusion systems have exploited an intuitive idea that a patterning instability is possible depending on the local environment, and, hence, one can think of *local* pointwise Turing conditions in order to determine where patterning will occur [37–41]. This research has also given rise to various multiscale approaches for analysis of mode coupling between spatial forcing and emergent Turing patterns [42–44]. However, as far as we are aware, no justification for this localization, or the use of canonical (trigonometric) unstable eigenmodes, has been given in the literature. Several authors have attempted to deduce Turing conditions in spatially forced reaction–diffusion equations [45–47], but these results are limited to special cases regarding asymptotic assumptions and nonlinear kinetics, and even the case of varying diffusion coefficients is not perfectly understood [48]. We note that Dewel & Borckmans [45] in particular analyse the case of slowly varying heterogeneity and employ a WBKJ-like ansatz, as we do below. However, their approach is substantially different from our own as they neglect the finite size of the domain, and do not recover the local Turing conditions that we seek, or the form of unstable modes.

Turing instabilities leading to pattern formation are typically considered to be induced due to the addition of diffusion (diffusion-driven instability) [5] and due to an increase in the domain-size [49]; below a certain critical domain size, patterns cannot be formed but above a minimal size, any small spatial perturbation of a reference homogeneous steady state will grow. The classical case focusing on spatially homogeneous systems is a textbook analysis and typically proceeds via a dispersion relation tying the Laplacian eigenmodes with the perturbation's growth rate [5,50–52]. However, as we shall show, justifying such a relationship between the growth rate and the operator's spectrum is much harder in the case of arbitrary spatial heterogeneity.

A major difficulty in analysing instabilities in systems with spatial heterogeneity is that there is no simple generalization of Sturm–Liouville theory to multiple-component systems [49]. One can make use of the scalar theory when the heterogeneity appears in the same way in each component and is scaled such that the spatial operator, including diffusion, is identical in each equation. However, more generally, such a theory is difficult to use and, at best, one finds existence results, or must resort to numerical approaches [53,54]. On the other hand, the WKBJ approximation has been employed in many optical and semi-classical quantum mechanical situations involving spatial heterogeneity [55–57], and, as we will demonstrate, has a straightforward generalization to coupled systems.

Here, we use WKBJ methods [58] in order to compute instability criteria for a reaction–diffusion system with explicit spatial heterogeneity in the kinetics, under the assumption that the heterogeneity is sufficiently smooth and not rapidly varying compared with the diffusive length scales. Our analysis also shows several novel aspects of these instabilities in the presence of heterogeneity, such as modes supported in different regions of the domain depending on their growth rates. This phenomenon invalidates some heuristics commonly employed in homogeneous Turing pattern formation, such as restricting analysis to the mode with the fastest growth rate, which in the heterogeneous case varies across the domain. These structural results can help explain size and wavelength modulation in the presence of heterogeneity observed both in simulations and heterogeneous environments in experiment.

We begin by setting up the system and reviewing conditions for a Turing instability in the homogeneous case, and stating the corresponding conditions in the spatially heterogeneous setting in §2. This section is a roadmap of our results and is intended to state the conditions without detailed derivation. Such a derivation is presented in §3, with the classical results in the homogeneous case in electronic supplementary material, S1. We end this section with a discussion of properties of these solutions, and how their form implies the instability conditions, with some technical details in electronic supplementary material, S2. In §4, we illustrate our results in the case of the Schnakenberg system, demonstrating both that our conditions for instability correspond to full numerical solutions, as well as showing various structural properties regarding the emergent unstable modes in line with our analysis. Finally, we discuss our results in §5, highlighting both applications of our method and future directions for extensions. Someone interested primarily in our results, rather than the technicalities of the WKBJ calculations, can skip §3, and instead just read §§2 and 4–5 to understand the implications of our results, as well as how to apply them to different systems.

2. Homogeneous and inhomogeneous instability conditions

Here, we state instability conditions for both homogeneous and heterogeneous two component reaction–diffusion systems that lead to emergent spatial patterning. In the heterogeneous setting, we exploit asymptotically small diffusion coefficients, and so pose the general problem first. We consider a dimensional two component system in one spatial dimension,

$$\mathbf{u}_t = \mathbf{D}_{\text{dim}}\mathbf{u}_{xx} + \mathbf{F}_{\text{dim}}(\mathbf{u}, x), \quad t > 0, \quad x \in (0, L),$$
$$\mathbf{D}_{\text{dim}} = \begin{pmatrix} D_1 & 0 \\ 0 & D_2 \end{pmatrix},$$

where $D_1 > D_2 > 0$ are the diffusion coefficients and L is the domain length. We prescribe Neumann boundary conditions ($\mathbf{u}_x = 0$ for $x \in \{0, L\}$) and the initial condition $\mathbf{u}(x, 0) = \mathbf{u}_0(x)$. We non-dimensionalize length scales with respect to L, timescales with respect to a reaction timescale T, and concentrations with respect to a typical concentration scale U for both components and diffusion coefficients by D_1. Reusing $\mathbf{u}$, t and x to now represent non-dimensional quantities for brevity we have

$$\begin{aligned} &\mathbf{u}_t = \varepsilon^2\mathbf{D}\mathbf{u}_{xx} + \mathbf{F}(\mathbf{u}, x), \quad t > 0, \quad x \in [0, 1], \\ &\varepsilon^2 = \frac{D_1 T}{L^2}, \quad \mathbf{D} = \begin{pmatrix} 1 & 0 \\ 0 & d \end{pmatrix}, \quad d = \frac{D_2}{D_1} \leq 1, \end{aligned} \tag{2.1}$$

where $\mathbf{F}(\mathbf{u}, x) = (f(\mathbf{u}, x), g(\mathbf{u}, x))$ is now a non-dimensional vector of kinetic functions. Below we assume $0 < \varepsilon \ll 1$. This asymptotic assumption is not physiologically unreasonable in developmental settings. Consider kinetic timescales of $T \sim 10$ min, the shortest that would allow for gene expression [59,60], a domain length of $L \sim 1$ mm and a diffusion coefficient of $D_1 \sim 9.4 \times 10^{-9}$ cm^2 s^{-1}, as measured in a synthetic biology experiment for the protein Lefty, the most mobile of the prospective developmental Turing morphogen pair Nodal and Lefty, as part of an investigation analysing Turing's mechanism in depth [61]. One then has $\varepsilon^2 \sim 5.6 \times 10^{-4}$ and hence $\varepsilon \sim 0.024$.

Let $\mathbf{u}^*(x)$ denote a steady state, so that

$$\mathbf{0} = \varepsilon^2 \mathbf{D}\mathbf{u}^*_{xx} + \mathbf{F}(\mathbf{u}^*, x), \quad x \in [0,1],$$

with boundary conditions $\mathbf{u}^*_x = 0$. To generalize the notion of a homogeneous steady state, we only consider the possibility that $\mathbf{u}^*$ oscillates with spatial derivatives of scale $O(1)$, or smaller, specifically excluding spatial oscillations on the scale of $O(1/\varepsilon)$, or larger. Hence, $\mathbf{u}^*$ is independent of ε and we have

$$\mathbf{0} = \mathbf{F}(\mathbf{u}^*, x) + O(\varepsilon^2), \tag{2.2}$$

as long as the spatial heterogeneity in $\mathbf{F}$ permits $\mathbf{u}^*_x = 0$ at $x = 0, 1$. If instead $\mathbf{u}^*_x \neq 0$ at either boundary then a boundary layer with concomitant large derivatives will form, a possibility that we neglect in the subsequent analysis. However, note that when the underlying heterogeneity is the result of prior patterning, as is the motivating background here, the steady state $\mathbf{u}^*$ will automatically be subject to the same zero flux boundary conditions unless the boundary fluxes change as one patterning mechanism progresses into the next. However, zero flux boundary conditions are ubiquitous in models of biological pattern formation [5] and hence requiring $\mathbf{u}^*_x = 0$ at $x = 0, 1$ does not constitute a particularly demanding constraint, at least in the context of hierarchical self-organization in developmental biology.

We proceed by linearizing about this steady state via $\mathbf{w} = \mathbf{u} - \mathbf{u}^*$, which is assumed small component-wise even relative to the scale of ε, to yield

$$\mathbf{w}_t = \varepsilon^2 \mathbf{D}\mathbf{w}_{xx} + \mathbf{J}(x)\mathbf{w}, \tag{2.3}$$

where $\mathbf{J}(x)$ is the Jacobian matrix of $\mathbf{F}$ evaluated at $\mathbf{u}^*(x)$. System (2.3) inherits homogeneous Neumann boundary conditions and the initial condition $\mathbf{w}(x, 0) = \mathbf{u}(x, 0) - \mathbf{u}^*(x)$. The fundamental impact of spatial heterogeneity in the kinetics is that the Jacobian $\mathbf{J}$ possesses an explicit spatial dependence (and formally an additional $O(\varepsilon^2)$ dependence, though we can neglect this via the asymptotic analysis going forward). The standard derivation in the homogeneous setting proceeds by assuming the ansatz $\mathbf{w} \propto e^{\lambda t}\mathbf{q}(x)$, justified by linearity. One then uses eigenvalues of the Laplacian to find $\lambda(n)$, where n is a spectral parameter, resulting in conditions which imply $\Re(\lambda) > 0$ and, hence, instability.

This approach does not generalize to the heterogeneous setting due to the explicit spatial dependence of $\mathbf{J}$, and so instead we think of varying λ as a parameter and searching for eigenvalues consistent with the form of the solution when $\Re(\lambda) > 0$. We first state a reformulation of the classical homogeneous conditions before generalizing to the heterogeneous case. We give a detailed rederivation in the homogeneous case in electronic supplementary material, S1, arriving at the following formulation of the Turing conditions:

Instability criterion 2.1 (homogeneous). *Let $0 < \varepsilon \ll 1$, and $\mathbf{J}$ a constant matrix for all $x \in [0, 1]$. If we assume stability to homogeneous perturbations, i.e.*

$$\mathrm{tr}(\mathbf{J}) < 0, \quad \det(\mathbf{J}) > 0, \tag{2.4}$$

then there exists a non-homogeneous perturbation $\mathbf{w}$ satisfying (2.3) which grows exponentially in time in the interval $x \in [0, 1]$ if

$$\mathrm{tr}(\mathbf{D}^{-1}\mathbf{J}) > 0, \quad [\mathrm{tr}(\mathbf{D}^{-1}\mathbf{J})]^2 - 4\det(\mathbf{D}^{-1}\mathbf{J}) > 0. \tag{2.5}$$

We find an analogous result in the spatially heterogeneous setting involving a much more complicated form of unstable modes explicitly depending on the growth rate λ, so that, to leading order, we have unstable solutions of the form $\mathbf{w} \propto e^{\lambda t}\mathbf{q}(x, \lambda)$. Additionally, for different growth rates λ, the instability may be restricted to different subsets of the spatial domain (asymptotically at leading order). We will denote the largest of these regions, within which we anticipate patterns to be confined, as $\mathcal{T}_0$, which can consist of multiple disjoint intervals (as in figure 1*h*). We denote the interior of this region as $\mathcal{T}_0^i$. Conditions for instability in the heterogeneous case then follow from criterion 3.9, and proposition 3.8, which are stated and derived in the next section. These conditions can be stated as

Instability criterion 2.2 (heterogeneous). *Let $0 < \varepsilon \ll 1$, and assume that the quantity $[\mathrm{tr}(\mathbf{D}^{-1}\mathbf{J}(x))]^2 - 4\det(\mathbf{D}^{-1}\mathbf{J}(x))$ has only simple zeros for $x \in [0, 1]$. If we assume stability to perturbations in the absence of diffusion, i.e.*

$$\mathrm{tr}(\mathbf{J}(x)) < 0, \quad \det(\mathbf{J}(x)) > 0, \text{ for all } x \in [0, 1], \tag{2.6}$$

then there exists a non-homogeneous perturbation $\mathbf{w}$ satisfying (2.3) (for sufficiently small ε and to leading order in ε) which grows exponentially in time for all $x \in \mathcal{T}_0^i$ if

$$\begin{aligned} &\mathrm{tr}(\mathbf{D}^{-1}\mathbf{J}(x)) > 0, \\ &[\mathrm{tr}(\mathbf{D}^{-1}\mathbf{J}(x))]^2 - 4\det(\mathbf{D}^{-1}\mathbf{J}(x)) > 0, \\ &\text{for all } x \in \mathcal{T}_0^i \end{aligned} \tag{2.7}$$

where $\mathcal{T}_0^i$ is the largest set for which conditions (2.7) hold.

More generally, the conditions of criterion 2.2 are exactly a local version of the homogeneous results, so that the same conditions satisfied on a subset of the full spatial domain imply a pattern forming instability on that subset. Both homogeneous and heterogeneous conditions hold for sufficiently small ε, which can be thought of as a sufficiently large spatial domain. In this case, one can neglect the discrete wave mode selection, though we do give discrete dispersion relations in electronic supplementary material, S1, for the homogeneous case, and criterion 3.9 for the heterogeneous case. These discrete conditions give concrete ways to determine precisely which modes become unstable, and their associated growth rates, for a fixed value of ε. In the next section, we will describe how to derive criterion 2.2 and these results mentioned above, and also further structural details about such instabilities which emerge from the form of unstable modes. One can skip these details on a first reading and see an illustration of the results in §4.

3. Deriving the spatially inhomogeneous conditions

We start our analysis of the heterogeneous Turing instability by analysing the stability of the steady state in line with the usual Turing instability analysis. We seek solutions to equation (2.3) in the form $\mathbf{w}(x, t) = e^{\lambda t}\mathbf{q}(x)$ (as linearity permits separability in t and x) to find

$$\mathbf{0} = \varepsilon^2 \mathbf{D}\mathbf{q}_{xx} + \mathbf{J}_\lambda(x)\mathbf{q}, \tag{3.1}$$

with $\mathbf{J}_\lambda = \mathbf{J} - \lambda\mathbf{I}$. We then proceed in direct analogy to the scalar WKBJ expansion [57,58], with

$$\mathbf{q} = \exp\left[\frac{i\varphi(x)}{\varepsilon}\right]\mathbf{p}(x) \quad \text{and}$$

$$\mathbf{p}(x) = \mathbf{p}_0(x) + \varepsilon\mathbf{p}_1(x) + \varepsilon^2\mathbf{p}_1(x) + \ldots.$$

Thus, with $'$ denoting the ordinary derivative with respect to x,

$$\begin{aligned}\mathbf{q}_{xx} &= \exp\left[\frac{i\varphi}{\varepsilon}\right]\left[\left(\frac{i\varphi'}{\varepsilon}\mathbf{p}+\mathbf{p}'\right)'+\frac{i\varphi'}{\varepsilon}\left(\frac{i\varphi'}{\varepsilon}\mathbf{p}+\mathbf{p}'\right)\right]\\ &= \exp\left[\frac{i\varphi}{\varepsilon}\right]\left[-\frac{\varphi'^2}{\varepsilon^2}\mathbf{p}+\frac{1}{\varepsilon}(2i\varphi'\mathbf{p}'+i\varphi''\mathbf{p})+\mathbf{p}''\right],\end{aligned}$$

and, hence,

$$\mathbf{0} = [-\varphi'^2\mathbf{D}+\mathbf{J}_\lambda]\mathbf{p}+\varepsilon[2i\varphi'\mathbf{D}\mathbf{p}'+i\varphi''\mathbf{D}\mathbf{p}]+O(\varepsilon^2),$$

where the $O(\varepsilon^2)$ terms from $\mathbf{J}$ were neglected, as we will not need to consider the second order problem below. At leading order in ε, we have

$$\mathbf{0} = [-\varphi'^2\mathbf{D}+\mathbf{J}_\lambda]\mathbf{p}_0 = \mathbf{D}[-\varphi'^2\mathbf{I}+\mathbf{B}_\lambda]\mathbf{p}_0,$$

where we define the matrix $\mathbf{B}_\lambda = \mathbf{D}^{-1}\mathbf{J}_\lambda = \mathbf{D}^{-1}(\mathbf{J}-\lambda\mathbf{I})$ and at next to leading order

$$\begin{aligned}\mathbf{0} &= [-\varphi'^2\mathbf{D}+\mathbf{J}_\lambda]\mathbf{p}_1+[2i\varphi'\mathbf{D}\mathbf{p}_0'+i\varphi''\mathbf{D}\mathbf{p}_0]\\ &= \mathbf{D}\{[-\varphi'^2\mathbf{I}+\mathbf{B}_\lambda]\mathbf{p}_1+[2i\varphi'\mathbf{p}_0'+i\varphi''\mathbf{p}_0]\}.\end{aligned}$$

We solve the leading-order equations by setting φ'^2 equal to an eigenvalue of $\mathbf{B}_\lambda$ and set $\mathbf{p}_0 = Q_0(x)\mathbf{p}_*(x)$ where $\mathbf{p}_*(x)$ is the unit magnitude eigenvector of $[-\varphi'^2\mathbf{I}+\mathbf{B}_\lambda]$ with zero eigenvalue and $Q_0(x)$ is an undetermined scalar function. Then

$$\begin{aligned}-[-\varphi'^2\mathbf{I}+\mathbf{B}_\lambda]\mathbf{p}_1 &= [2i\varphi'\mathbf{p}_0'+i\varphi''\mathbf{p}_0]\\ &= i[2\varphi'Q_0'+\varphi''Q_0]\mathbf{p}_*+2i\varphi'Q_0\mathbf{p}_*'.\end{aligned}$$

The matrix premultiplying $\mathbf{p}_1$ has zero determinant and hence the existence of a solution requires a solvability condition.

Let $\mathbf{s}_*^T(x)$ be the zero left eigenvector of unit magnitude of $[-\varphi'^2\mathbf{I}+\mathbf{B}_\lambda]$. Then we have the solvability condition $\mathbf{s}_*^T(x)[-\varphi'^2\mathbf{I}+\mathbf{B}_\lambda]=\mathbf{0}$ by Fredholm's alternative, and thus multiplying by $\mathbf{s}_*^T(x)$ we have

$$[2\varphi'Q_0'+\varphi''Q_0]\mathbf{s}_*{}^T\mathbf{p}_*+2\varphi'Q_0\mathbf{s}_*{}^T\mathbf{p}_*'=0, \tag{3.2}$$

which yields

$$\frac{Q_0'}{Q_0} = -\frac{\varphi''}{2\varphi'}-\frac{\mathbf{s}_*{}^T\mathbf{p}_*'}{\mathbf{s}_*{}^T\mathbf{p}_*}.$$

Thus

$$Q_0(x) = \frac{Q_{00}}{\sqrt{\varphi'}}\exp\left[-\int_a^x\frac{\mathbf{s}_*(\bar{x})^T\mathbf{p}_*'(\bar{x})}{\mathbf{s}_*(\bar{x})^T\mathbf{p}_*(\bar{x})}\,\mathrm{d}\bar{x}\right], \tag{3.3}$$

where Q_{00} is a constant, not necessarily real, φ' is given by either the positive or the negative square root of the eigenvalues of $\mathbf{B}_\lambda$, and a is an arbitrary real constant before any constraints of considering real solutions and the boundary conditions are imposed. Hence, for each eigenvalue of $\mathbf{B}_\lambda(x)$, denoted

$$\mu_\lambda^\pm(x) \equiv \varphi'^2(x),$$

we have a possible mode which, at leading order, can be written as

$$\begin{aligned}\mathbf{w}(x,t) = \mathrm{e}^{\lambda t}&\exp\left[-\int_a^x\frac{\mathbf{s}_*(\bar{x})^T\mathbf{p}_*'(\bar{x})}{\mathbf{s}_*(\bar{x})^T\mathbf{p}_*(\bar{x})}\,\mathrm{d}\bar{x}\right]\frac{1}{[\mu_\lambda^\pm]^{1/4}(x)}\\ &\times\left\{C_0^\pm\cos\left[\frac{1}{\varepsilon}\int_a^x\sqrt{\mu_\lambda^\pm(\bar{x})}\,\mathrm{d}\bar{x}\right]\right.\\ &\left.+S_0^\pm\sin\left[\frac{1}{\varepsilon}\int_a^x\sqrt{\mu_\lambda^\pm(\bar{x})}\,\mathrm{d}\bar{x}\right]\right\}\mathbf{p}_*(x),\end{aligned} \tag{3.4}$$

where $C_0^\pm$, $S_0^\pm$ are arbitrary constants. We note that the reciprocal of ε from the trigonometric functions will dominate in spatial derivatives given our asymptotic assumptions.

In the usual Turing analysis, we assume that the steady state is stable to homogeneous perturbations, which are associated with the zero mode. By analogy, we therefore seek stability to perturbations which have spatial derivatives of, at most, the same O(1) scale as the steady state, in contrast to the WKBJ modes in equation (3.4), where spatial derivatives scale with $1/\varepsilon$, due to the $1/\varepsilon$ factors in the trigonometric contributions. Solutions with the required behaviour are found by setting $\varphi=0$ in the WKBJ expansion or, equivalently by considering $\mathbf{w}(x,t)=\mathrm{e}^{\lambda t}\mathbf{q}(x)$ with a *regular* perturbation expansion for $\mathbf{q}(x)$. One finds $\mathbf{J}_\lambda(x)\mathbf{q}(x)=\mathbf{0}$ at leading order and hence the derivatives of $\mathbf{q}(x)$ are independent of ε and thus order unity at this level of approximation. Hence, for such solutions, substituting $\mathbf{w}(x,t)=\mathrm{e}^{\lambda t}\mathbf{q}(x)$ into equation (2.3) reduces to

$$\mathbf{w}_t = \varepsilon^2\mathbf{D}\mathbf{w}_{xx}+\mathbf{J}(x)\mathbf{w}\approx\mathbf{J}(x)\mathbf{w}, \tag{3.5}$$

since $|\mathbf{w}_{xx}|\sim O(1)$ for this kind of perturbation. Stability of the equilibrium to such perturbations is required for all x and thus, to asymptotic accuracy, we require

$$\begin{aligned}&\mathrm{tr}(\mathbf{J}(x)) = f_u+g_v<0,\\ &\det(\mathbf{J}(x)) = f_ug_v-f_vg_u>0,\\ &\text{for all } x\in\mathcal{T}_0^i\end{aligned} \tag{3.6}$$

a set of two constraints that we shall assume throughout the text below. These conditions generalize the notion of stability against homogeneous perturbation in the spatially homogeneous setting, and imply that any unstable mode of the form (3.4) will lead to emergent spatial patterning that is not strictly dictated by the spatial heterogeneity in the kinetics.

The above expression for the leading-order solution $\mathbf{w}$ is well defined with the exception of zeros of $\mu_\lambda^\pm$ (which we will show can be excluded in proposition 3.6 below) and potential singular points $x_*\in[0,1]$ where $\mathbf{s}_*{}^T\mathbf{p}_*=0$. These singular points will in fact determine the subsets of the spatial domain in which a patterning instability will occur. We first consider properties of λ and $\mu_\lambda^\pm$, independently from the solution structure given by (3.4), in an arbitrary interval $(a,b)\subset[0,1]$, and then discuss how to choose such an interval so that solutions can be defined. After this, we discuss how solutions behave near these singular points in order to define solutions globally in space. Note, in particular, that we will restrict attention to the open interval (a,b), as we will eventually choose these boundaries to (possibly) be singular points.

3.1. Local Turing conditions

Motivated by the form of solution (3.4), we now consider the quantities λ and $\mu_\lambda^\pm$ in their own right, and deduce properties that these quantities must have to make sense of such a solution. If the WKBJ solution, (3.4), is defined everywhere on the domain $x\in[0,1]$, Neumann boundary conditions at the domain edges entail, at leading order in ε, that the integral

$$\int_0^1\sqrt{\mu_\lambda^\pm(\bar{x})}\,\mathrm{d}\bar{x} \tag{3.7}$$

is a multiple of $\pi\varepsilon/2$ and, without loss, $a=S_0^\pm=0$ so that only cosine solutions remain. Furthermore, given the choice of a sufficiently small ε, the above constraint can be ensured

simply by imposing

$$\int_0^1 \sqrt{\mu_\lambda^\pm(\bar{x})}\,\mathrm{d}\bar{x} \in \mathbb{R} \setminus \{0\}. \tag{3.8}$$

However, we are not guaranteed that the WKBJ solution, (3.4), is defined everywhere on the domain $x \in [0, 1]$. In general, the region of validity for the WKBJ solution will be restricted to one or more intervals of the form (a, b) where a and b are constants satisfying $0 \le a < b \le 1$. The pathological case of a region of validity that is restricted to a point is neglected, as this requires mathematical precision in the parameter values. As discussed in §3.2, when the WKBJ solutions are not valid everywhere, homogeneous Dirichlet boundary conditions will be required (i.e. whenever a, b satisfy $a > 0$ or $b < 1$). Given sufficiently small ε, as discussed immediately above, then we may accommodate both cases of homogeneous boundary conditions, Neumann or Dirichlet, by requiring (i) without loss a restriction of the WKBJ solution to either a sine or a cosine by setting either $C_0^\pm = 0$ or $S_0^\pm = 0$ to guarantee the boundary condition at $x = a$ and (ii)

$$\int_a^b \sqrt{\mu_\lambda^\pm(\bar{x})}\,\mathrm{d}\bar{x} \in \mathbb{R} \setminus \{0\}, \tag{3.9}$$

for $0 \le a < b \le 1$ so that the integral in (3.9) can be guaranteed to be a multiple of either $\pi\varepsilon$ or $\pi\varepsilon/2$ for a suitable, sufficiently small, choice of ε to guarantee the homogeneous boundary condition at $x = b$.

From the fundamental constraint (3.9), we can deduce properties of λ and $\mu_\lambda^\pm$ that are necessary for a solution to exist within an arbitrary region of validity, (a, b), with $\Re(\lambda) > 0$, therefore resulting in a perturbation that grows in amplitude. An analogous derivation in the spatially homogeneous setting is given in electronic supplementary material, S1, and is the motivation for what follows. Critically, we assume that conditions (3.6) hold for every proposition below. We remark that here we derive implications directly from the fundamental constraint (3.9) that will let us make sense of solutions of the form given in (3.4), but do not assume *a priori* that such solutions must be valid.

We first define *permissible* growth rates and eigenvalues which satisfy (3.9).

Definition 3.1. A permissible pair $(\lambda, \mu_\lambda^\pm(x))$ is such that the value of λ entails $\mu_\lambda^\pm(x)$ satisfies constraint (3.9) for all x in some interval (a, b).

We will also refer to λ as permissible, or $\mu_\lambda^\pm(x)$ as permissible, if $(\lambda, \mu_\lambda^\pm(x))$ is permissible, as defined above, and implicitly assume this is over an interval (a, b).

Proposition 3.2. *The function $\mu_\lambda^\pm(x)$ is permissible if and only if $\mu_\lambda^\pm(x)$ is real and non-negative for all $x \in (a, b)$, though not identically zero. Additionally, without loss of generality we can consider the integral in (3.9) to be positive.*

Proof. If $\mu_\lambda^\pm(x)$ is real, non-negative and not identically zero for $x \in (a, b)$ it is immediate that it is permissible. For the converse, we consider a permissible $\mu_\lambda^\pm(x)$. Note that the square root in condition (3.9) is, without loss of generality, the positive square root. In other words, we work in the complex plane such that any argument, denoted θ below, is in the range $\theta \in [0, 2\pi)$ and the positive square root is such that if, for example, $\theta/2 \in [0, \pi)$, then

$$(\mathrm{e}^{i\theta})^{1/2} = \mathrm{e}^{i\theta/2}.$$

Hence, any imaginary contribution to the integrand, $\sqrt{\mu_\lambda^\pm(x)}$, in condition (3.9) is non-negative as the argument of the square root in the complex plane is in the range $[0, \pi)$. So any imaginary contribution to the integrand cannot be cancelled from a contribution in any other region of the integration domain. Thus, the integrand cannot have an imaginary contribution and $\sqrt{\mu_\lambda^\pm(x)}$ must be real for all $x \in (a, b)$. Hence, $\mu_\lambda^\pm(x)$ is real and non-negative for all $x \in (a, b)$. Finally, the need for the integral to not be identically zero implies that $\mu_\lambda^\pm(x)$ cannot be identically zero. □

Proposition 3.3. *If λ is both permissible and complex (i.e. $\Im(\lambda) \neq 0$), then $\Re(\lambda) < 0$.*

Proof. From the definition of $\mu_\lambda^\pm(x)$, we have

$$\det[-\mu_\lambda^\pm(x)\mathbf{D} + \mathbf{J}_\lambda(x)] = 0,$$

and, so,

$$\begin{aligned} 2\lambda = -\mathrm{tr}(\mu_\lambda^\pm(x)\mathbf{D} - \mathbf{J}) \pm \sqrt{[\mathrm{tr}(\mu_\lambda^\pm(x)\mathbf{D} - \mathbf{J})]^2 - 4\det[\mu_\lambda^\pm(x)\mathbf{D} - \mathbf{J}]} = [f_u + g_v - \mu_\lambda^\pm(x)(1+d)] \\ \pm \sqrt{(f_u + g_v - \mu_\lambda^\pm(x)(1+d))^2 - 4(d(\mu_\lambda^\pm(x))^2 - (df_u + g_v)\mu_\lambda^\pm(x) + (f_u g_v - g_u f_v))}, \end{aligned} \tag{3.10}$$

with the spatial dependence of $\mu_\lambda^\pm(x)$ such that the growth rate, λ, does not have a dependence on x. Given λ is permissible, so that $\mu_\lambda^\pm(x)$ is permissible, we have that $\mu_\lambda^\pm(x)$ is real and non-negative for all $x \in (a, b)$. In addition, $\mathrm{tr}(\mathbf{J}) = f_u + g_v < 0$ for all x by equation (3.6) implying that $f_u + g_v - \mu_\lambda^\pm(x)(1+d) < 0$ and, thus, if a permissible λ is complex it has a negative real part. □

Proposition 3.4. *Given $\Re(\lambda) \ge 0$, the pair $(\lambda, \mu_\lambda^\pm(x))$ is permissible if and only if*

$$\mathrm{tr}(\mathbf{B}_\lambda) > 0 \quad \text{and} \quad [\mathrm{tr}(\mathbf{B}_\lambda)]^2 - 4\det(\mathbf{B}_\lambda) \ge 0, \tag{3.11}$$

for all $x \in (a, b)$.

Proof. If $(\lambda, \mu_\lambda^\pm(x))$ is permissible, with $\Re(\lambda) \ge 0$, then λ is real by proposition 3.3. From permissibility and proposition 3.2 we also have $\mu_\lambda^\pm(x)$ is real, non-negative and not identically zero for all $x \in (a, b)$. From $\det(-\mu_\lambda^\pm(x)\mathbf{D} + \mathbf{J}_\lambda(x)) = 0$, we have

$$\mu_\lambda^\pm(x) = \frac{1}{2}\left[\mathrm{tr}(\mathbf{B}_\lambda) \pm \sqrt{[\mathrm{tr}(\mathbf{B}_\lambda)]^2 - 4\det(\mathbf{B}_\lambda)}\right]. \tag{3.12}$$

As $\mu_\lambda^\pm(x)$ and λ are strictly real, this enforces

$$[\mathrm{tr}(\mathbf{B}_\lambda)]^2 - 4\det(\mathbf{B}_\lambda) \ge 0,$$

for all $x \in (a, b)$. We also have

$$\det(\mathbf{B}_\lambda) = \det(\mathbf{D}^{-1}\mathbf{J}_\lambda) = \det(\mathbf{D}^{-1})$$
$$\det(\mathbf{J}_\lambda) = \det(\mathbf{J}_\lambda)/d > 0$$

for all $x \in (a, b)$, using equation (3.6) and that λ is real and non-negative. Hence, for both the positive and negative square root in equation (3.12), the fact that $\mu_\lambda^\pm(x)$ cannot be negative enforces $\mathrm{tr}(\mathbf{B}_\lambda) \geq 0$ for all $x \in (a, b)$. The possibility that $\mathrm{tr}(\mathbf{B}_\lambda) = 0$ is excluded as then $\mu_\lambda^\pm(x)$ is not real, since $\det(\mathbf{B}_\lambda) > 0$.

Conversely, assuming conditions (3.11), we can see by equation (3.12) that $\mu_\lambda^\pm(x) > 0$ for all $x \in (a, b)$, and, hence, condition (3.9) is satisfied. □

We note that conditions (3.11) cannot be satisfied in the case $d = 1$, as then $\mathrm{tr}(\mathbf{B}_\lambda) = \mathrm{tr}(\mathbf{J}) - 2\lambda < \mathrm{tr}(\mathbf{J}) < 0$, so for any permissible λ with $\Re(\lambda) > 0$, we must have $d < 1$. As the conditions in (3.11) do not depend on the positive or negative branch of $\mu_\lambda^\pm$, we immediately have that this proposition implies both roots are permissible once one of them is. We also need the following proposition, which shows that if these conditions hold for $\lambda > 0$, then they hold for $\lambda = 0$.

Proposition 3.5. *If the conditions* (3.11) *hold for some real permissible* λ^* *with* $\lambda^* > 0$ *for all* $x \in (a, b)$, *then they hold for all real* λ *with* $\lambda^* \geq \lambda \geq 0$ *for all* $x \in (a, b)$.

Proof. First, we realize that $\mathrm{tr}(\mathbf{B}_\lambda) = \mathrm{tr}(\mathbf{B}_0) - \lambda(1 + 1/d)$, and the last term is strictly negative so that from $\mathrm{tr}(\mathbf{B}_{\lambda^*}) > 0$ we have $\mathrm{tr}(\mathbf{B}_\lambda) > 0$ for all $0 \leq \lambda \leq \lambda^*$. Next, we consider the second condition of (3.11), which can be written as

$$P(\lambda) := \left(1 - \frac{1}{d}\right)^2 \lambda^2 - \frac{2(d-1)(df_u - g_v)}{d^2}\lambda + \left(f_u + \frac{g_v}{d}\right)^2 - 4\frac{f_u g_v - f_v g_u}{d} \geq 0, \tag{3.13}$$

where the quadratic $P(\lambda)$ admits two zeros, which we can compute as

$$\tilde{\lambda}^\pm = \frac{g_v - df_u \pm 2\sqrt{-df_v g_u}}{1 - d}.$$

We can see that these roots are both real by signing each term. From $\mathrm{tr}(\mathbf{J}) < 0$ while $\mathrm{tr}(\mathbf{B}_{\lambda^*}) = \mathrm{tr}(\mathbf{D}^{-1}\mathbf{J}_{\lambda^*}) > 0$ for $\lambda^* > 0$ we have that $f_u + g_v < 0$ while $f_u + g_v/d > 0$ and $d < 1$. Hence $f_u < 0$, $g_v > 0$ and $f_u - g_v/d < 0$.

Due to the positive coefficient of λ^2 in $P(\lambda)$, we can see that this function must have a negative minimum, so that it is positive to the left of $\tilde{\lambda}^-$ and to the right of $\tilde{\lambda}^+$ (and negative between these roots). If $\lambda^* \leq \tilde{\lambda}^-$, then $P(\lambda)$ is decreasing in λ and, so, $P(\lambda) > 0$ for all $0 \leq \lambda \leq \lambda^*$, meaning that we would be done. Hence, we now assume that $\lambda^* \geq \tilde{\lambda}^+$ to derive a contradiction. By linearity we have $0 < \mathrm{tr}(\mathbf{B}_{\lambda^*}) \leq \mathrm{tr}(\mathbf{B}_{\tilde{\lambda}^+})$. We then compute,

$$\mathrm{tr}(\mathbf{B}_{\tilde{\lambda}^+}) = \frac{-(2d+2)\sqrt{-df_v g_u} + 2d(f_u - g_v)}{(1-d)d} < 0,$$

which can be seen as the denominator is strictly positive and the numerator has only negative terms. Therefore, we must have $\lambda^* \leq \tilde{\lambda}^-$, so that $P(\lambda) \geq 0$ for all $\lambda < \lambda^*$. □

Next we show a relationship between the positive and negative eigenvalues of $\mathbf{B}_\lambda$, and how they depend on λ. We will need to assume that $[\mathrm{tr}(\mathbf{B}_\lambda)]^2 - 4\det(\mathbf{B}_\lambda) > 0$ for all $x \in (a, b)$. If this term becomes zero (and hence $\mu_\lambda^-(x) = \mu_\lambda^+(x)$), then there is a degeneracy in the associated eigenvectors, which will lead to an internal boundary-layer behaviour discussed in the next section, and hence the determination of the boundary points, a and b.

Proposition 3.6. *Given* $(\lambda, \mu_\lambda^\pm(x))$ *is permissible,* $\Re(\lambda) > 0$, *and* $[\mathrm{tr}(\mathbf{B}_\lambda)]^2 - 4\det(\mathbf{B}_\lambda) > 0$ *for all* $x \in (a, b)$, *we then have the ordering* $0 < \mu_0^-(x) < \mu_\lambda^-(x) < \mu_\lambda^+(x) < \mu_0^+(x)$ *for all* $x \in (a, b)$. *Furthermore, at the edges of the domain,* $x = a$, *or* $x = b$, *we still have the ordering* $0 < \mu_0^-(x) \leq \mu_\lambda^-(x) \leq \mu_\lambda^+(x) \leq \mu_0^+(x)$.

Proof. Using ∂_λ to denote differentiation with respect to λ, we have that $\partial_\lambda \mathrm{tr}(\mathbf{B}_\lambda) = -\mathrm{tr}(\mathbf{D}^{-1}) = -(1 + 1/d)$ and $\partial_\lambda \det(\mathbf{B}_\lambda) = -\mathrm{tr}(\mathbf{J}_\lambda)/d = (2\lambda - f_u - g_v)/d$. Then, by equation (3.12), $(\mu_\lambda^\pm(x))^2 - \mathrm{tr}(\mathbf{B}_\lambda)\mu_\lambda^\pm(x) + \det(\mathbf{B}_\lambda) = 0$, so, upon taking the derivative and rearranging we have,

$$\partial_\lambda \mu_\lambda^\pm(x) = \frac{-d\mathrm{tr}(\mathbf{D}^{-1})\mu_\lambda^\pm(x) + \mathrm{tr}(\mathbf{J}_\lambda)}{d(2\mu_\lambda^\pm(x) - \mathrm{tr}(\mathbf{B}_\lambda))} = \frac{-d\mathrm{tr}(\mathbf{D}^{-1})\mu_\lambda^\pm(x) + \mathrm{tr}(\mathbf{J}_\lambda)}{\pm d\sqrt{[\mathrm{tr}(\mathbf{B}_\lambda)]^2 - 4\det(\mathbf{B}_\lambda)}}. \tag{3.14}$$

We can then see that each term in the numerator is always negative for both roots, whereas the denominator will change sign. Hence, we have $\partial_\lambda \mu_\lambda^-(x) > 0$ and $\partial_\lambda \mu_\lambda^+(x) < 0$, so that the ordering follows by continuity. Finally, we note that the possibility of $\mu_0^- \leq 0$ is excluded using equation (3.12) along with proposition 3.2 and $\mathrm{tr}(\mathbf{B}_0) > 0$, the latter of which is true by virtue of proposition 3.5.

For the second part, all of the ordering can be deduced as a limit of the above argument (with the new potential equality $\mu_\lambda^- = \mu_\lambda^+$ if $[\mathrm{tr}(\mathbf{B}_0)]^2 - 4\det(\mathbf{B}_0) = 0$ by equation (3.12)) except the definite inequality $\mu_0^- > 0$. To rule out $\mu_0^- = 0$, we consider $\lambda = 0$. If $[\mathrm{tr}(\mathbf{B}_0)]^2 - 4\det(\mathbf{B}_0) > 0$ at the boundary point as well, the above proof holds. Hence we need now only consider the case with $[\mathrm{tr}(\mathbf{B}_0)]^2 - 4\det(\mathbf{B}_0) = 0$. Now suppose, for contradiction, that $\mu_0^- = 0$. By (3.12) we have $\mathrm{tr}(\mathbf{B}_0) = 0$ and hence $\det(\mathbf{B}_0) = \det(\mathbf{J})/d = 0$, but we have $\det(\mathbf{J}) > 0$ throughout, and hence the contradiction. □

Propositions 3.5 and 3.6 together give a range of permissible values of λ and associated eigenvalues $\mu_\lambda^\pm$, as soon as the conditions (3.11) are satisfied for some positive $\lambda^* > 0$. Finally, we show that for a permissible λ with $\Re(\lambda) \geq 0$, and the same assumption as above, we can sensibly define the left and right eigenvectors $\mathbf{s}_*$ and $\mathbf{p}_*$ which are not orthogonal.

Proposition 3.7. *Given* $(\lambda, \mu_\lambda^\pm(x))$ *is permissible and* $\Re(\lambda) \geq 0$, *then* $[\mathrm{tr}(\mathbf{B}_\lambda)]^2 - 4\det(\mathbf{B}_\lambda) > 0$ *for all* $x \in (a, b)$ *if and only if* $\mathbf{s}_*^T\mathbf{p}_* \neq 0$ *for all* $x \in (a, b)$, *where* $\mathbf{s}_*$ *and* $\mathbf{p}_*$ *are the left and right unit eigenvectors of* $[-\mu_\lambda^\pm\mathbf{I} + \mathbf{B}_\lambda]$.

Proof. We will demonstrate both implications via contraposition. We first assume that $\mathbf{s}_*^T\mathbf{p}_* = 0$ at some point $x_* \in (a, b)$. By elaborating possibilities on a case by case basis for a general 2×2 matrix with zero determinant, we note the left and right eigenvectors of zero eigenvalue can only be perpendicular if the matrix is proportional to one of the following:

$$\begin{pmatrix} 0 & 0 \\ 0 & 0 \end{pmatrix}, \quad \begin{pmatrix} 1 & 1 \\ -1 & -1 \end{pmatrix}, \begin{pmatrix} 1 & -1 \\ 1 & -1 \end{pmatrix}.$$

In all three cases, we have that the trace is zero. Therefore, $\mathrm{tr}(-\mu_\lambda^\pm \mathbf{I} + \mathbf{B}_\lambda) = -2\mu_\lambda^\pm + \mathrm{tr}(\mathbf{B}_\lambda) = 0$. However, by equation (3.12), this implies that $[\mathrm{tr}(\mathbf{B}_\lambda)]^2 - 4\det(\mathbf{B}_\lambda) = 0$, contradicting the assumption that this quantity remains positive.

For the converse, we assume that $[\mathrm{tr}(\mathbf{B}_\lambda)]^2 - 4\det(\mathbf{B}_\lambda) = 0$ at some point $x_* \in (a, b)$ (noting that if this term were negative, then, by proposition 3.4, λ would not be permissible and we would have an immediate contradiction). By using equation (3.12) again we see that $\mathrm{tr}(-\mu_\lambda^\pm \mathbf{I} + \mathbf{B}_\lambda) = 0$, so this matrix then has repeated zero eigenvalues. Any real 2×2 matrix with zero determinant and trace can be written as either,

$$\begin{pmatrix} c_1 & c_2 \\ -\frac{c_1^2}{c_2} & -c_1 \end{pmatrix}, \quad \text{or} \quad \begin{pmatrix} 0 & 0 \\ 0 & 0 \end{pmatrix},$$

for real c_1, c_2, with $c_2 \neq 0$. The first of these has one left and one right eigenvector, given by $\mathbf{s}_* = (c_1/c_2, 1)$ and $\mathbf{p}_* = (-c_2/c_1, 1)$, which are orthogonal. The second of these would imply $f_v = g_u = 0$, and, along with the assumption that $\det(\mathbf{J}) > 0$, we would have $f_u g_v > 0$, so these terms must have the same sign. But noting that $\mathrm{tr}(\mathbf{J}) < 0$ and $\mathrm{tr}(\mathbf{B}_\lambda) > 0$, by assumption on the stability of the zero mode, permissibility of λ, and proposition 3.4, we have $f_u + g_v < 0$ and $f_u + g_v/d - \lambda/d > 0$, thus, we see that they must have opposite signs, demonstrating that this case is not possible. Therefore, if $[\mathrm{tr}(\mathbf{B}_\lambda)]^2 - 4\det(\mathbf{B}_\lambda) = 0$ at some point $x_* \in (a, b)$ for permissible λ, then $\mathbf{s}_*^T \mathbf{p}_* = 0$ at this point. □

Given propositions 3.4, 3.6 and 3.7, which all follow from the definition of permissible growth rates, we can now consider where solutions of the form given in equation (3.4) for permissible $\lambda \geq 0$ are valid. We will assume throughout that $[\mathrm{tr}(\mathbf{B}_\lambda)]^2 - 4\det(\mathbf{B}_\lambda)$ only has simple zeros, noting that non-simple zeros would require mathematical fine tuning of parameters. When $[\mathrm{tr}(\mathbf{B}_\lambda)]^2 - 4\det(\mathbf{B}_\lambda) \geq 0$, we have by the first part of proposition 3.6 that the reciprocal of $[\mu_\lambda^\pm]^{1/4}$ with permissible $\lambda \geq 0$ is non-singular and thus equation (3.4) with permissible $\lambda \geq 0$ might only possess a singularity at points where left and right eigenvectors are orthogonal, that is $\mathbf{s}_*^T \mathbf{p}_* = 0$. Then, for a region with $\mathrm{tr}(\mathbf{B}_\lambda) > 0$, and $[\mathrm{tr}(\mathbf{B}_\lambda)]^2 - 4\det(\mathbf{B}_\lambda) \geq 0$ we have that λ is permissible by proposition 3.4 and that the reciprocal of $[\mu_\lambda^\pm]^{1/4}$ is non-singular, even at the domain edges by the additional use of the second part of proposition 3.6. We define the closure of the maximal open set where the associated WKBJ solution for this λ is non-singular by $\mathcal{T}_\lambda$. By the above reasoning and proposition 3.7 each boundary of this region must either be a domain boundary, or where $[\mathrm{tr}(\mathbf{B}_\lambda)]^2 - 4\det(\mathbf{B}_\lambda) = 0$ as $\mathbf{s}_*^T \mathbf{p}_* \neq 0$ on the interior of $\mathcal{T}_\lambda$. Whenever the latter case occurs, $\mathcal{T}_\lambda \neq [0, 1]$ and we have to determine what happens to the WKBJ solution on approaching the point where $\mathbf{s}_*^T \mathbf{p}_* \neq 0$ and beyond.

3.2. Behaviour near singular points

If $\mathcal{T}_\lambda = [0, 1]$, for a given permissible $\lambda \geq 0$, then we can take $a = S_0^\pm = 0$ in (3.4) to find a non-trivial solution that satisfies the homogeneous Neumann boundary conditions. If instead $\mathcal{T}_\lambda$ is a proper subset of the whole interval [0, 1] then we assume for simplicity that $\mathcal{T}_\lambda$ is a single contiguous interval, implying that $[\mathrm{tr}(\mathbf{B}_\lambda)]^2 - 4\det(\mathbf{B}_\lambda)$ has at most two zeros for $x \in [0, 1]$, and note that generalizing beyond a single interval is straightforward. At a zero of $[\mathrm{tr}(\mathbf{B}_\lambda)]^2 - 4\det(\mathbf{B}_\lambda)$, by (3.12) we have the double eigenvalues, $\mu_\lambda^- = \mu_\lambda^+$, of $\mathbf{B}_\lambda$ and we recap that by proposition 3.7 we have $\mathbf{s}_*^T \mathbf{p}_* = 0$ at such a point, denoted x_*, and thus anticipate a singularity in the solution given by equation (3.4). In electronic supplementary material, S2, we explicitly show that for $y > x > x_*$ the integral

$$\exp\left[\int_x^y \frac{\mathbf{s}_*(\bar{x}) \cdot \mathbf{p}_*'(\bar{x})}{\mathbf{s}_*(\bar{x}) \cdot \mathbf{p}_*(\bar{x})}\, \mathrm{d}\bar{x}\right], \tag{3.15}$$

will blow up as $x \searrow x_*$, with analogous behaviour when approaching such a singular point from the left. However, in this electronic supplementary material section, we also show that this integral will scale such that by imposing effective Dirichlet conditions at the singular point, we can retain a bounded solution. In this way, we can construct leading-order solutions which are bounded and defined on $\mathcal{T}_\lambda$.

With the previously stated assumption that any zero of $[\mathrm{tr}(\mathbf{B}_\lambda)]^2 - 4\det(\mathbf{B}_\lambda)$ is simple, so that $[\mathrm{tr}(\mathbf{B}_\lambda)]^2 - 4\det(\mathbf{B}_\lambda)$ monotonically passes through zero at such a singular point and by proposition 3.7 we thus have that $[\mathrm{tr}(\mathbf{B}_\lambda)]^2 - 4\det(\mathbf{B}_\lambda) < 0$ outside of $\mathcal{T}_\lambda$. By proposition 3.4, this implies that this value of λ is not permissible outside of this interval, and hence if any WKBJ solutions exist, they cannot simultaneously satisfy homogeneous Dirichlet or Neumann conditions at boundaries on both the left and right. However, the scaling of the integral (3.15) requires a solution that is zero at the singular point, while a zero derivative is always required at a domain boundary. Thus the only WKBJ solution outside of $\mathcal{T}_\lambda$ associated with the growth rate λ is the zero solution. We can then extend the non-trivial WKBJ solution defined on $\mathcal{T}_\lambda$ by the zero solution to obtain a leading-order solution across the whole domain for a mode with fixed growth rate λ.

We can now match these different sets of boundary conditions depending on the number of singular points appearing in the domain. These will then lead to different wavenumber selection conditions. We note in particular that in matching Neumann boundaries, we only differentiate the trigonometric functions in (3.4), as only terms involving these derivatives will be retained to leading order. We then have the following leading-order solutions (modes) associated with each eigenvalue $\mu_\lambda^\pm$ of $\mathbf{B}_\lambda = \mathbf{D}^{-1}\mathbf{J}_\lambda(x)$, depending on the number of singular points:

— no singular points, so $\mathcal{T}_\lambda = [0, 1]$ and the solution is

$$\left.\begin{aligned} \mathbf{w}^\pm(x, t) = {} & \mathrm{e}^{\lambda t} \exp\left[-\int_0^x \frac{\mathbf{s}_*(\bar{x})^T \mathbf{p}_*'(\bar{x})}{\mathbf{s}_*(\bar{x})^T \mathbf{p}_*(\bar{x})}\, \mathrm{d}\bar{x}\right] \\ & \times \frac{C_0^\pm}{[\mu_\lambda^\pm(x)]^{1/4}} \cos\left(\frac{1}{\varepsilon}\int_0^x \sqrt{\mu_\lambda^\pm(\bar{x})}\, \mathrm{d}\bar{x}\right) \mathbf{p}_*(x) \\ \text{and} \quad & \int_0^1 \sqrt{\mu_\lambda^\pm(\bar{x})}\, \mathrm{d}\bar{x} = n^\pm \pi\varepsilon; \end{aligned}\right\} \tag{3.16a}$$

— one singular point $x_*(\lambda) > 0$, so without loss of generality, $(x_*, 1) = \mathcal{T}_\lambda$, with solution

$$\left.\begin{aligned} \mathbf{w}^\pm(x, t) = {} & \mathrm{e}^{\lambda t} \exp\left[\int_x^1 \frac{\mathbf{s}_*(\bar{x})^T \mathbf{p}_*'(\bar{x})}{\mathbf{s}_*(\bar{x})^T \mathbf{p}_*(\bar{x})}\, \mathrm{d}\bar{x}\right] \frac{S_0^\pm}{[\mu_\lambda^\pm(x)]^{1/4}} \\ & \times \sin\left(\frac{1}{\varepsilon}\int_{x_*}^x \sqrt{\mu_\lambda^\pm(\bar{x})}\, \mathrm{d}\bar{x}\right) \mathbf{p}_*(x) \\ \text{and} \quad & \int_{x_*}^1 \sqrt{\mu_\lambda^\pm(\bar{x})}\, \mathrm{d}\bar{x} = \left(n^\pm + \frac{1}{2}\right)\pi\varepsilon, \end{aligned}\right\} \tag{3.16b}$$

for $x \in \mathcal{T}_\lambda$, and zero otherwise;

— two singular points $x_*(\lambda), x_{**}(\lambda) \in (0, 1)$ delimiting the $\mathcal{T}_\lambda$ set, i.e. $\mathcal{T}_\lambda = (x_*, x_{**})$, with solution

$$\left.\begin{aligned} \mathbf{w}^{\pm}(x,t) &= \mathrm{e}^{\lambda t}\exp\left[\int_x^{x_{**}} \frac{\mathbf{s}_*(\bar{x})^T\mathbf{p}_*'(\bar{x})}{\mathbf{s}_*(\bar{x})^T\mathbf{p}_*(\bar{x})}\,\mathrm{d}\bar{x}\right]\frac{S_0^{\pm}}{[\mu_\lambda^{\pm}(x)]^{1/4}} \\ &\quad\times\sin\left(\frac{1}{\varepsilon}\int_x^{x_{**}}\sqrt{\mu_\lambda^{\pm}(\bar{x})}\,\mathrm{d}\bar{x}\right)\mathbf{p}_*(x) \\ \text{and}\quad &\int_{x_*(\lambda)}^{x_{**}(\lambda)}\sqrt{\mu_\lambda^{\pm}(\bar{x})}\,\mathrm{d}\bar{x} = n^{\pm}\pi\varepsilon, \end{aligned}\right\} \tag{3.16c}$$

for $x \in \mathcal{T}_\lambda$, and zero otherwise;

where $C_0^{\pm}, S_0^{\pm}$ are arbitrary real constants. We remark that the mode selection constraint is defined over $\mathcal{T}_\lambda$, and so will depend on λ through both the eigenvalues $\mu_\lambda^{\pm}$ and any singularities, as highlighted in the integral bounds. In this way, the latter two solutions given by equations (3.16*b*)–(3.16*c*) are continuously extended by zero outside of $\mathcal{T}_\lambda$, and equal to zero at the singular points.

We remark that these WKBJ solutions applied to systems without heterogeneity in the reaction kinetics collapse in both components to functions of the form

$$\mathrm{e}^{\lambda t}(C_0\cos(n\pi x) + S_0\sin(n\pi x)).$$

However, the meaning of n (denoted as $n^{\pm}$) in the heterogeneous case does not correspond to the spatial frequency of a given mode, as we will see in an example. We can now describe some additional structural features of the spaces $\mathcal{T}_\lambda$ and how they change for different growth rates λ. In particular, the set $\mathcal{T}_\lambda$ is monotonic in λ in the following sense.

Proposition 3.8. *If $\mathcal{T}_{\lambda_2} \neq \emptyset$ and $0 \le \lambda_1 \le \lambda_2$ then $\mathcal{T}_{\lambda_2} \subseteq \mathcal{T}_{\lambda_1}$. If $\mathcal{T}_{\lambda_1} \neq [0, 1]$, and $0 \le \lambda_1 < \lambda_2$, then we have the stricter inclusion $\mathcal{T}_{\lambda_2} \subset \mathcal{T}_{\lambda_1}$.*

Proof. The first part of this for $0 \le \lambda_1 \le \lambda_2$ follows from proposition 3.5. We then need to show that if $\lambda_1 < \lambda_2$, then $\mathcal{T}_{\lambda_1} \not\subseteq \mathcal{T}_{\lambda_2}$. We note that at least one of the boundaries of $\mathcal{T}_\lambda$, $a(\lambda)$ and/or $b(\lambda)$, are zeros (in the spatial variable x) of $\mathrm{tr}(\mathbf{B}_\lambda(x))^2 - 4\det(\mathbf{B}_\lambda(x))$. At such a boundary, we compute the derivative with respect to λ, finding

$$\begin{aligned} &\partial_\lambda[(\mathrm{tr}(\mathbf{B}_\lambda(x))^2 - 4\det(\mathbf{B}_\lambda(x))] \\ &\quad = -2\mathrm{tr}(\mathbf{B}_\lambda)\mathrm{tr}(\mathbf{D}^{-1}) + 4\mathrm{tr}(\mathbf{J}_\lambda)\det(\mathbf{D}^{-1}) < 0, \end{aligned} \tag{3.17}$$

which follows by signing each term. As $\mathrm{tr}(\mathbf{B}_\lambda(x))^2 - 4\det(\mathbf{B}_\lambda(x)) > 0$ for $a(\lambda) < x < b(\lambda)$, we have that if $a(\lambda_1) > 0$ then $a(\lambda_1) < a(\lambda_2)$ and if $b(\lambda_1) < 1$ then $b(\lambda_1) > b(\lambda_2)$, so the strict inclusion $\mathcal{T}_{\lambda_2} \subset \mathcal{T}_{\lambda_1}$ follows. □

Hence, the onset of instability (the boundary of $\mathcal{T}_0$) is given by zeros of $[\mathrm{tr}(\mathbf{B}_0)]^2 - 4\det(\mathbf{B}_0) = 0$, for which $\mathrm{tr}(\mathbf{B}_0) > 0$. More generally, the onset of instability with a growth rate $\lambda \ge 0$ is given by the location of zeros of $\mathbf{s}_*^T\mathbf{p}_* = 0$, i.e. zeros of $[\mathrm{tr}(\mathbf{B}_\lambda)]^2 - 4\det(\mathbf{B}_\lambda) = 0$ while $\mathrm{tr}(\mathbf{B}_\lambda > 0)$. Therefore, this boundary shifts with λ, while monotonicity of the $\mathcal{T}_\lambda$ with respect to λ holds. Hence, the sufficient condition for (the onset of) instability can be identified with $\mathcal{T}_0$, which is a good approximation of where we will find Turing patterns, as it corresponds to the region of support of a mode with positive value of λ for sufficiently small ε. This also justifies considering the fundamental constraint (3.9) in this regime, which does not depend on ε.

In summary, we have the following conditions for instability:

Instability criterion 3.9 (λ-dependent heterogeneous case). *Let $\lambda > 0$, $0 < \varepsilon \ll 1$, and assume that the quantity $[\mathrm{tr}(\mathbf{B}_\lambda(x))]^2 - 4\det(\mathbf{B}_\lambda(x))$ has no more than two simple zeros for $x \in [0, 1]$, and is positive between these two zeros. If we assume stability to perturbations in the absence of diffusion, i.e.*

$$\mathrm{tr}(\mathbf{J}(x)) < 0, \quad \det(\mathbf{J}(x)) > 0, \text{ for all } x \in [0, 1], \tag{3.18}$$

then there exists a non-homogeneous perturbation $\mathbf{w}$ satisfying (2.3) (to leading order in ε) which grows as $\mathrm{e}^{\lambda t}$ in the interval $x \in (a(\lambda), b(\lambda))$ if

$$\begin{aligned} &\mathrm{tr}(\mathbf{B}_\lambda(x)) > 0, \quad [\mathrm{tr}(\mathbf{B}_\lambda(x))]^2 - 4\det(\mathbf{B}_\lambda(x)) > 0, \\ &\text{for all } x \in (a(\lambda), b(\lambda)), \end{aligned} \tag{3.19}$$

and if there exists an integer $n^{\pm} > 0$ such that

$$\int_{a(\lambda)}^{b(\lambda)}\sqrt{\mu_\lambda^{\pm}(\bar{x})}\,\mathrm{d}\bar{x} = \left(n^{\pm} + \frac{K}{2}\right)\pi\varepsilon, \tag{3.20}$$

where $a(\lambda) = \max(0,\ \min(\{x : [\mathrm{tr}(\mathbf{B}_\lambda(x))]^2 - 4\det(\mathbf{B}_\lambda(x)) = 0\}))$, $b(\lambda) = \min(1,\ \max(\{x : [\mathrm{tr}(\mathbf{B}_\lambda(x))]^2 - 4\det(\mathbf{B}_\lambda(x)) = 0\}))$ and $K = 0$ if either $a(\lambda) = 0$ and $b(\lambda) = 1$, or if $0 < a(\lambda) < b(\lambda) < 1$; otherwise $K = 1$.

Proof. We assume without loss of generality that $(a(\lambda), b(\lambda))$ has one of the forms given in (3.16). By proposition 3.3 we have no loss in specializing to strictly real λ. Assuming conditions (3.19) are satisfied, propositions 3.2 and 3.4 imply that $\mu_\lambda^{\pm}$ is permissible, real, and positive. From this and proposition 9 (electronic supplementary material, S2), we have that the functions given by (3.16) are real and bounded for all $x \in (a(\lambda), b(\lambda))$. To leading order in ε, such solutions satisfy (2.3), alongside the zero solution. By the scaling arguments in electronic supplementary material, S2, we can see that the solutions given by (3.16) meet this zero solution at any internal boundary (i.e. any zero of $[\mathrm{tr}(\mathbf{B}_\lambda(x))]^2 - 4\det(\mathbf{B}_\lambda(x))$ in the interval $(0, 1)$). So to leading order, such a piecewise solution satisfies (2.3) and the Neumann boundary conditions at $\{0, 1\}$. □

Analogous criteria for the other possibilities for $\mathcal{T}_\lambda$, depending on the sign pattern of $[\mathrm{tr}(\mathbf{B}_\lambda(x))]^2 - 4\det(\mathbf{B}_\lambda(x))$ across the domain, are readily determined. Furthermore, we note that the integers $n^{\pm}$ play an analogous role to the wavenumber n in the homogeneous setting, but that they will not correspond to spatial frequency, and the two roots will have quantitatively different properties, so must be considered as distinct. For sufficiently small ε, these conditions predict that a pattern will form in the interval (a, b), and intervals for which no value of λ exists will return to the heterogeneous steady-state $\mathbf{u}^*$ after a small perturbation (up to leading order in ε). We will confirm this numerically in §4. Additionally, the fact that unstable modes do not share the same support is shown explicitly in proposition 3.8, and employed to explain some properties of patterns in heterogeneous domains.

We remark that (3.20) depends on a given λ both in the integrand and the bounds of the integral, but in principle for a given ε and $n^{\pm}$, one can use this condition to find at most two values of λ indicating an instability, one for each eigenvalue. Hence, any instability will permit a discrete number of

unstable modes, each with a possibly different support, and the growth rate of any instability will, thus, depend locally on the permissible growth rates. We give further structural details regarding $n^{\pm}$ and λ in electronic supplementary material, S3.

Further, it should be noted that criterion 3.9 can be generalized to obtain criterion 2.2 by relaxing the restriction to a single interval, and considering a suitable choice of arbitrarily small ε. The use of the interior of $\mathcal{T}_0$ in this limit for criterion 2.2 is further supported by proposition 3.8, and noting that instabilities need not grow on the edges of $\mathcal{T}_0$ for the WKBJ solutions at leading order (in particular this is the case when the homogeneous Dirichlet boundary conditions are imposed to retain bounded solutions there). However, although linked, we highlight that criterions 2.2 and 3.9 are different. Criterion 3.9 gives conditions for the presence of a specific unstable WKBJ Turing mode, which is subject to the wavemode selection relation of equation (3.20). Aside from a trivial relaxation of the requirement that the WKBJ Turing mode may only have support within a single interval, criterion 2.2 gives conditions that ensure that there is at least one destabilizing WKBJ Turing mode with a positive growth rate for sufficiently small ε, effectively by amalgamating criterion 3.9 across all possible modes. Hence, criterion 2.2 is the most useful in classifying whether or not there is a Turing instability. Nonetheless, criterion 3.9 is a fundamental stepping stone to deriving criterion 2.2 and, in addition, provides detailed information, for example, about the location of the support of the WKBJ Turing mode solutions and the relation between the growth rate to the non-dimensional diffusion coefficient, via equation (3.20).

4. Illustrative example. The Schnakenberg model

To illustrate our results, we consider the Schnakenberg model with spatially heterogeneous sources. Let

$$\mathbf{u} = \begin{pmatrix} u_1 \\ u_2 \end{pmatrix},$$

so that u_1 is the nominal inhibitor and u_2 is the nominal activator. The kinetics are

$$\mathbf{F}(\mathbf{u}, x) = \begin{pmatrix} \beta(x) - u_2^2 u_1 \\ u_2^2 u_1 - \alpha u_2 + \zeta(x) \end{pmatrix},$$

with $\alpha, \beta(x), \zeta(x) > 0$. As is typical, and to simplify the system, we assume $\beta(x) + \zeta(x) = 1$. Hence, accurate to $O(\varepsilon^2)$, the steady state is given by

$$\mathbf{u}^* = \begin{pmatrix} \alpha^2 \beta(x) \\ \frac{1}{\alpha} \end{pmatrix},$$

Note that $\mathbf{u}^*(x)$ has no dependence on ε at this order of approximation by construction and furthermore $\beta(x)$ is taken so that $\mathbf{u}^*(x)$ satisfies the boundary conditions at the domain edges, as required in the derivation of equation (2.2) and discussed in detail in §2. We proceed by evaluating the Jacobian, which is given by

$$\mathbf{J} = \left(\begin{array}{c|c} -\frac{1}{\alpha^2} & -2\alpha\beta(x) \\ \hline \frac{1}{\alpha^2} & \alpha(2\beta(x) - 1) \end{array} \right),$$

so that

$$\left.\begin{aligned} \mathrm{tr}(\mathbf{J}) = \alpha(2\beta(x) - 1) - \frac{1}{\alpha^2}, \quad \det(\mathbf{J}) = \frac{1}{\alpha}, \quad \mathrm{tr}(\mathbf{D}^{-1}\mathbf{J}) = \frac{\alpha}{d}(2\beta(x) - 1) - \frac{1}{\alpha^2} \\ \text{and} \quad [\mathrm{tr}(\mathbf{D}^{-1}\mathbf{J})]^2 - 4\det(\mathbf{D}^{-1}\mathbf{J}) = \frac{(2\beta(x) - 1)^2\alpha^6 + (-4\beta(x) - 2)d\alpha^3 + d^2}{\alpha^4 d^2}. \end{aligned}\right\} \tag{4.1}$$

We first note that the second constraint of the Turing condition, equation (3.18), is automatically satisfied since $\det(\mathbf{J}) > 1$. To satisfy the Turing conditions (3.19) for $\lambda = 0$ we require

$$4\alpha^6\beta(x)^2 - 4(\alpha^6 + \alpha^3 d)\beta(x) + \alpha^6 - 2\alpha^3 d + d^2 > 0 \tag{4.2a}$$

and

$$\beta(x) > \frac{1}{2}\left(1 + \frac{d}{\alpha^3}\right), \quad \beta(x) < \frac{1}{2}\left(1 + \frac{1}{\alpha^3}\right). \tag{4.2b}$$

Thus, inequalities (4.2*b*) require $d < 1$, as standard. Condition (4.2*a*) forces $\beta(x)$ to lie outside of the roots of this quadratic, i.e.

$$\beta(x) > \frac{1}{2}\left(1 + \frac{d}{\alpha^3}\right) + \sqrt{\frac{d}{\alpha^3}} \quad \text{or } \beta(x) < \frac{1}{2}\left(1 + \frac{d}{\alpha^3}\right) - \sqrt{\frac{d}{\alpha^3}}.$$

The second of these inequalities cannot be reconciled with the first inequality of (4.2*b*). We then have the conditions on the parameters for a Turing instability (at the marginal case of $\lambda = 0$) are that $\alpha > 0$, $0 < d < 1$, and for all $x \in \mathcal{T}_0$,

$$\frac{1}{2}\left(1 + \frac{d}{\alpha^3}\right) + \sqrt{\frac{d}{\alpha^3}} < \beta(x) < \frac{1}{2}\left(1 + \frac{1}{\alpha^3}\right),$$

with the latter inequality also enforcing the first constraint of the Turing condition, equation (3.18). The above inequality is also accompanied by the need to ensure an unstable mode satisfies condition (3.20), analogous to the *a posteriori* selection of a wavenumber for the spatially homogeneous Turing instability. This condition will be satisfied if and when the boundary conditions are satisfied.

4.1. Direct numerical solutions

We simulated system (2.1) with the Schnakenberg kinetics. Initial data were taken as normally distributed spatial perturbations to $\mathbf{u}^*$. Specifically, we set $u_i(0) = u_i^*(1 + \xi_i(x))$ where $i = 1, 2$ and $\xi_i(x) \sim \mathcal{N}(0, 10^{-3})$ independently for each x and i. While such heterogeneous reaction–diffusion systems are standard problems for numerical simulation software, we carefully checked different implementations of our simulations in order to be sure we resolved boundary layers and solution structure in the spatial domain. The commercial finite-element solver Comsol v. 5.4 was used to solve the equations with 10^5 elements, a relative tolerance of 10^{-4}, and a final time of $t = 10^6$ by which time a steady state had been reached up to numerical tolerances. Simulations were also carried out using a standard three-point stencil in MATLAB and the stiff solver *ode15s*, using 10^4 grid points with relative and absolute tolerances of 10^{-9}, and the same solutions were found. WKBJ modes were reconstructed in Mathematica and these were checked in MATLAB and Maple.

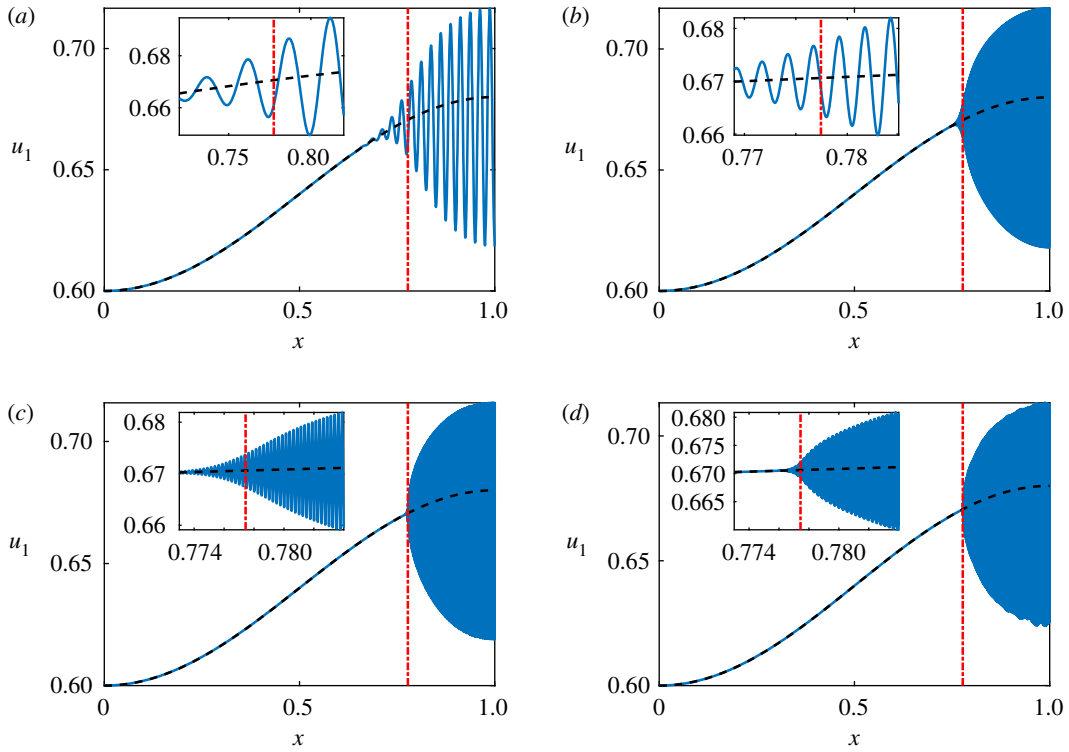

Figure 2. Plots of u_1 from simulations of the Schnakenberg system using $\alpha = 1$, $d = 1/40 = 0.025$, and $\beta = 3/5 + [1 - \cos(\pi x)]/25$ with varying ε. The blue solid curve is from the numerical simulation whereas the black dashed curve is the stationary state $u_1^*(x) = \beta(x)$ (note that the blue *region* is due to the highly oscillatory nature of the solution). The red dash-dotted curve is the boundary of $\mathcal{T}_0$ at $x \approx 0.7774$ (i.e. the singular point x_*). The insets show a zoomed-in region near the boundary of $\mathcal{T}_0$; these insets are over different regions in (*a*) and (*b*), though (*c*) and (*d*) share the same *x*-axis for their insets. (*a*) $\varepsilon = 10^{-2}$, (*b*) $\varepsilon = 10^{-3}$, (*c*) $\varepsilon = 10^{-4}$, (*d*) $\varepsilon = 10^{-5}$. (Online version in colour.)

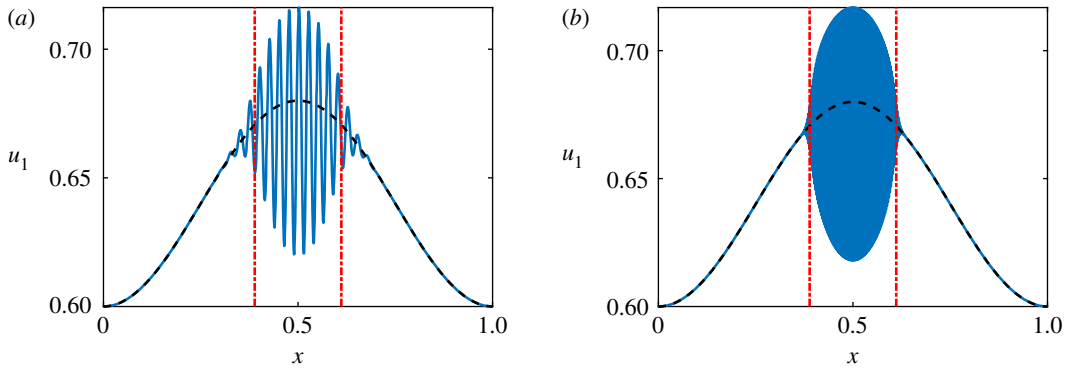

Figure 3. Plots of u_1 as in figure 2, but with $\beta = 3/5 + [1 - \cos(2\pi x)]/25$ to demonstrate an internally contained $\mathcal{T}_0$. (*a*) $\varepsilon = 10^{-2}$, (*b*) $\varepsilon = 10^{-3}$. (Online version in colour.)

We demonstrate our results using the following parameter choices, unless otherwise stated. We take $\alpha = 1$, $d = 1/40 = 0.025$, and consider $\beta = 3/5 + [1 - \cos(c\pi x)]/25$, where $c = 1$ or $c = 2$. For these parameters, we have a Turing instability if $0.6706 < \beta(x) < 1$, so for $c = 1$ we have $\mathcal{T}_0 \approx (0.7774, 1)$ and for $c = 2$ we have $\mathcal{T}_0 \approx (0.3886, 0.6114)$. We plot simulations for $c = 1$ in figure 2, and vary ε. We observe that patterned solutions form approximately in the region predicted by the analysis, $\mathcal{T}_0$, and that they localize to this region as ε is decreased with highly oscillatory boundary regions at $x_* \approx 0.7774$. We note that figures 2*b–d* have the same qualitative structure in terms of the amplitudes of patterns, though the internal oscillations become increasingly finer as ε is decreased. The insets show the increasing localization of the boundary as ε is decreased, as well as the structure of the decaying boundary layer of the mode with the largest support. We also show the same kind of localization for $c = 2$ in figure 3 where the spike solutions are confined to an internal region by varying the heterogeneity. Larger values of c, as well as other kinds of heterogeneity, were also considered with results consistent with the analytical predictions.

In figure 4, we show short time solutions to the nonlinear and linearized system in order to understand the structure of growing modes due to the instability. As anticipated, for sufficiently small perturbations and time intervals, the linear and nonlinear simulations are almost identical (using the same realization of the initial perturbations). We observe that the instability grows fastest furthest to the right, suggesting that there is not a single largest growth rate λ across the domain, as anticipated in the analysis. Rather, what we have plotted are a superposition of modes with

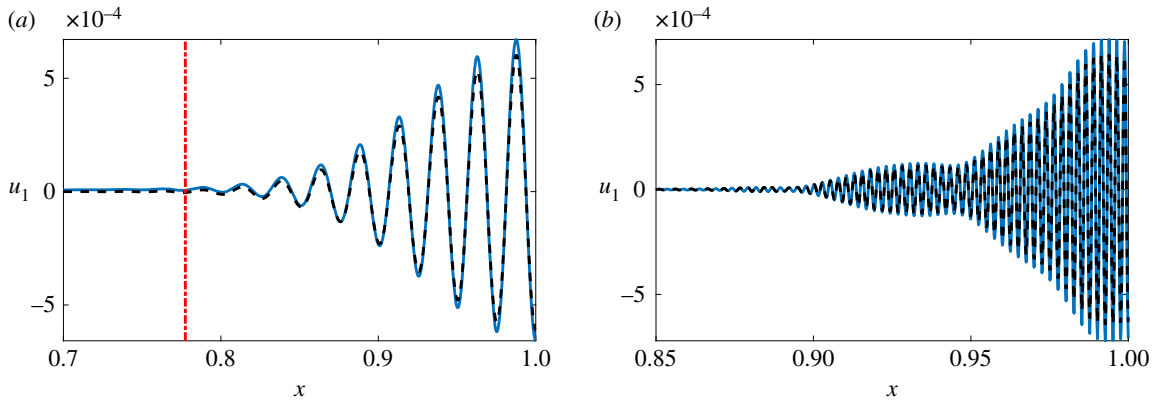

Figure 4. Plots of u_1 from simulations of the Schnakenberg system using $\alpha = 1$, $d = 1/40 = 0.025$, and $\beta = 3/5 + [1 - \cos(\pi x)]/25$ with varying ε at a times $t_f = 800$ in (*a*) and $t_f = 700$ in (*b*). The initial perturbation is taken as $\xi_i(x) \sim \mathcal{N}(0, 10^{-6})$ in both cases. The blue solid curve is given by $u_1(t_f) - u_1^*$ from the full numerical simulation, and the black dashed curve is given by $w_1(t_f)$ from simulations of the linearized system. The red dash-dotted curve is the boundary of $\mathcal{T}_0$ at $x \approx 0.7774$, though the region shown in (*b*) is entirely within $\mathcal{T}_0$. (*a*) $\varepsilon = 10^{-2}$, (*b*) $\varepsilon = 10^{-3}$. (Online version in colour.)

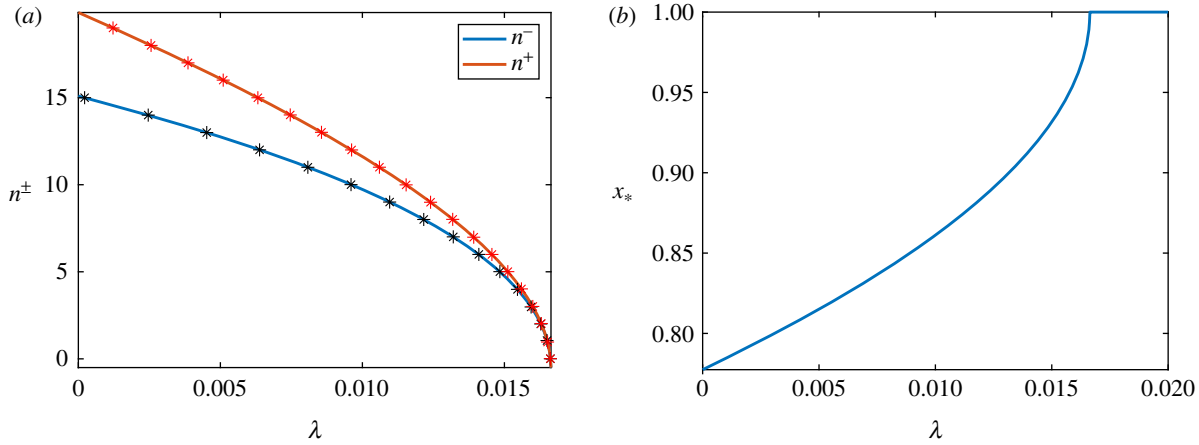

Figure 5. Evaluating (3.20) reveals the possible discrete modes $n^{\pm}$ on both branches of WKBJ solutions, which are plotted using asterisks in (*a*). In (*b*), we plot the position of singular points $x_*(\lambda)$ demarcating the boundary of $\mathcal{T}_\lambda = [x_*, 1]$ as a function of the growth rate λ, and corresponding to a shrinking $\mathcal{T}_\lambda$ which vanishes when $x_* = 1$. (Online version in colour.)

distinct growth rates and supports. Finally, for smaller ε, these results suggest that larger values of λ (which are more localized) become permissible, which is consistent with the structures anticipated. We now explore these modes in more detail.

4.2. Structure of unstable modes

We construct the unstable modes given by (3.16b) for the example shown in figure 2*a* with $\varepsilon = 0.01$, and discuss their properties. First, we numerically determine the discrete plausible mode numbers $n^{\pm} \in \mathbb{N}$ and λ from the constraint (3.20). Then $\mathbf{B}_\lambda$, $\mathbf{p}_*$, $\mathbf{s}_*$, μ_λ and $\mathbf{w}$ all follow from their definitions. This example is indicative of the general features of linearly unstable modes in heterogeneous reaction–diffusion systems; the restriction to an example with modes of the form given by (3.16b) is just for clarity of presentation, and our qualitative observations generalize. Specifically, unstable regions $\mathcal{T}_\lambda$ which are composed of many disjoint intervals will in general have a wide variety of unstable modes across the domain, but the analysis in any such complicated setting will essentially reduce to the structures found here.

In this particular example there are 19 unstable WKBJ eigenmodes on the branch corresponding to μ_λ^+ and 15 on the branch corresponding to μ_λ^-, all of which follow from computing λ from (3.20) as shown in figure 5*a*. Note that the right-most value of $n^{\pm}$ (here shown as a continuous interpolation) corresponds to $\lambda = 0$, i.e. the boundary of $\mathcal{T}_0$, and that indeed the first unstable WKBJ mode (on the negative branch in this particular example) appears near this boundary as predicted due to the small values of ε. We depict four of these modes from each branch in figure 6, noting that they each have a support which increases with n. We also see in figure 5*a* how the growth rate is related to the discrete values of n, and how the support of a corresponding mode changes with its growth rate λ in figure 5*b*. Figure 5 directly evidences the predictions from proposition 3.8 and the results in electronic supplementary material, section S3, as we see the support of distinct modes decrease with increasing λ. Finally, we remark that the vector $\mathbf{p}^*$ in equation (3.4) (computed numerically) is negative in its first component, and positive in its second (as expected for a cross-kinetic system like Schnakenberg), and both components are essentially constant in space, varying by less than 1% of their magnitude across the domain.

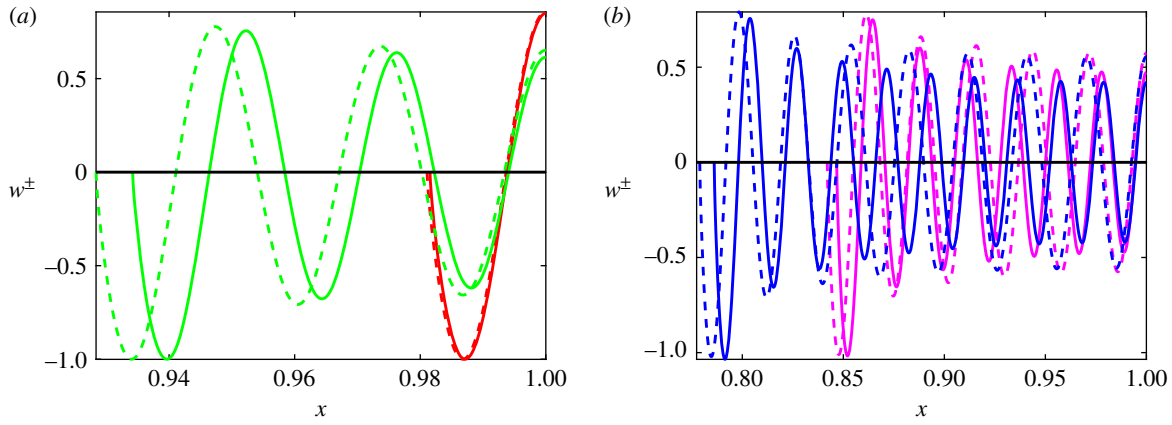

Figure 6. We plot the first component of modes given by (3.16*b*), associated with u_1, corresponding to parameters as in figure 2*a*. We plot modes for the positive branch μ_λ^+ (solid lines), with $n^+ = 1, 5, 13, 19$ in red, green, purple and blue, respectively, as well as the modes corresponding to the negative branch μ_λ^- (dashed lines), with $n^- = 1, 5, 11, 15$ in red, green, purple, and blue respectively. The smaller two mode numbers are shown in (*a*), and the larger two in (*b*). We remark that the smallest and largest values of $n^\pm$ correspond to the maximal and minimal mode numbers along each branch, and the other two mode numbers for each branch are chosen to have similar values of λ. Note the shrinkage of the support of each mode with increasing n, and in particular the difference in the axes for each plot. (Online version in colour.)

5. Discussion

We have analysed two-component heterogeneous reaction–diffusion systems in order to justify the use of *local* Turing conditions which are commonly employed in the literature, and given a deeper insight into how heterogeneity changes the structure of patterned states. Using a WKBJ ansatz, we have shown that *local* conditions are valid, provided that the heterogeneity is slowly varying. Additionally, we demonstrated that these unstable modes are supported in distinct regions of the domain with different growth rates, and without a well-defined wavenumber; this leads to the commonly observed amplitude variations reported in the literature. This is in contrast to the homogeneous case, where the pattern modes have a well-defined wavenumber and occupy the whole space (figure 1*b*). We illustrated our analytical predictions using a simple model in §4. Much more complicated heterogeneities and reaction–diffusion systems, such as those explored in [28] were also used to verify the analytical predictions in more complicated cases, such as when $\mathcal{T}_0$ is no longer a single interval. Nevertheless, the instability criteria work well for suitably small ε such that the heterogeneity does not vary faster than $O(1/\varepsilon)$. While we can enumerate the unstable modes and compute their growth rates, we remark that there is no obvious generalization of wavelength or frequency in this setting; unstable modes, and fully developed patterns, tend to exhibit large varying oscillations throughout a heterogeneous region of space.

Alongside generalizing the classical Turing conditions to the case of spatially heterogeneous systems, our analysis suggests several further questions to pursue. We have assumed that the local steady state is stable in the absence of diffusion throughout the domain, but it may be possible that diffusion could in fact *stabilize* the solution of a heterogeneous reaction–diffusion system which is locally unstable (in the absence of diffusion) in only part of its domain, leading to a patterned state. Additionally, it is known that rapidly varying heterogeneities can substantially impact the ability of a reaction–diffusion system to admit patterns, and the qualitative features that such patterns exhibit [36,41], and this remains to be explored within the present framework. Finally, while the results in electronic supplementary material, S3, allow us to conjecture about the envelope of solutions via the growth rate of distinct unstable modes, these remarks have not been rigorously justified. Demonstrating properties of these envelopes mathematically would require extending the framework of weakly nonlinear analysis [3,62–65] to the heterogeneous setting, and is beyond the scope of this paper.

In addition to these mathematical extensions, one could apply these results directly to biological patterning situations, such as successive patterning due to reaction–diffusion mechanisms on different timescales, or to the combination of theories of positional information and reaction–diffusion (figure 1). Originally, the well-known Gierer–Meinhardt model developed in [66] contained a spatial heterogeneity representing a precursor pattern from a previous pattern forming event. Such a situation could be directly captured by considering distinct reaction–diffusion processes occurring at different time points in development, or on different temporal and spatial scales. Alternatively, one can posit a positional information framework as the origination of spatial structure, such as in delineating different patterning fields from one another, and let reaction–diffusion theory produce additional periodic patterning within this heterogeneous domain, as suggested in [6]. Hence this paper presents a first step toward theoretically understanding the evolution of one pattern into another, but much more work must be done linking to experimental studies to justify such a theory of morphogenesis.

While the WKBJ-based approach we have employed is potentially extendable to multi-species or multi-dimensional systems, the calculations become increasingly complicated. Real chemical and biological systems are composed of many different chemical species, and few developmental phenomena are faithfully captured by a single spatial dimension. Additionally, we remark that our analysis presented in electronic supplementary material, S2, only shows that continuous modes can be defined across singularities at leading order, though fully resolving the boundary-layer structure across these singularities is beyond our present scope. Nevertheless, the results we have presented here will remain valid even with such refinements. We also anticipate

that these results are indicative of Turing instabilities in heterogeneous systems in higher dimensions, or with three or more species. Specifically, spatial regions which satisfy local Turing conditions should admit patterned solutions (distinct from the ambient heterogeneity) if these regions are sufficiently large, and the spatial heterogeneity is sufficiently smooth. Preliminary numerical investigations in two and three dimensions suggest this is true, and a valuable extension given the biological motivations for the theory. The framework presented here is a first step in understanding how one patterned state arises from another, and in elucidating the more nuanced roles that reaction and diffusion play in development and analogous systems with heterogeneous instabilities. As Turing said, though under different circumstances [67], 'We can only see a short distance ahead, but we can see plenty there that needs to be done.'

Data accessibility. In compliance with BBSRC's open access initiative, the data in this paper are available from https://doi.org/10.5287/bodleian:PPxMeZMDz.

Competing interests. We declare we have no competing interests.

Funding. A.L.K. and E.A.G. are grateful for support from BBSRC grant no. BB/N006097/1; V.K. is grateful for support from European Regional Development Fund-Project 'Center for Advanced Applied Science' (no. CZ.02.1.01/0.0/0.0/16_019/0000778) and the Mathematical Institute at the University of Oxford.

References

1. Turing AM. 1952 The chemical basis of morphogenesis. *Phil. Trans. R Soc. Lond. B* **237**, 37–72. (doi:10.1098/rstb.1952.0012)
2. De Kepper P, Castets V, Dulos E, Boissonade J. 1991 Turing-type chemical patterns in the chlorite–iodide–malonic acid reaction. *Physica D* **49**, 161–169. (doi:10.1016/0167-2789(91)90204-M)
3. Cross MC, Hohenberg PC. 1993 Pattern formation outside of equilibrium. *Rev. Mod. Phys.* **65**, 851–1112. (doi:10.1103/RevModPhys.65.851)
4. Kondo S, Miura T. 2010 Reaction–diffusion model as a framework for understanding biological pattern formation. *Science* **329**, 1616–1620. (doi:10.1126/science.1179047)
5. Murray JD. 2004 *Mathematical biology, interdisciplinary applied mathematics*. New York, NY: Springer.
6. Green JBA, Sharpe J. 2015 Positional information and reaction–diffusion: two big ideas in developmental biology combine. *Development* **142**, 1203–1211. (doi:10.1242/dev.114991)
7. Woolley T. 2014 Mighty morphogenesis. In *50 Visions of mathematics* (ed. S Parc), pp. 180–183. Oxford, UK: Oxford University Press.
8. Sheth R, Marcon L, Bastida MF, Junco M, Quintana L, Dahn R, Kmita M, Sharpe J, Ros MA. 2012 Hox genes regulate digit patterning by controlling the wavelength of a Turing-type mechanism. *Science* **338**, 1476–1480. (doi:10.1126/science.1226804)
9. Wolpert L. 2016 Positional information and pattern formation. In *Current topics in developmental biology*, vol. 117, pp. 597–608. London, UK: Academic Press.
10. Holloway DM. 1995 Reaction-diffusion theory of vertebrate organogenesis. PhD thesis, University of British Columbia.
11. Warmflash A, Sorre B, Etoc F, Siggia ED, Brivanlou AH. 2014 A method to recapitulate early embryonic spatial patterning in human embryonic stem cells. *Nat. Methods* **11**, 847–854. (doi:10.1038/nmeth.3016)
12. Weber EL, Woolley TE, Yeh C-Y, Ou K-L, Maini PK, Chuong C-M. 2019 Self-organizing hair peg-like structures from dissociated skin progenitor cells: new insights for human hair follicle organoid engineering and Turing patterning in an asymmetric morphogenetic field. *Exp. Dermatol.* **28**, 355–366. (doi:10.1111/exd.13891)
13. Meinhardt H. 1983 Cell determination boundaries as organizing regions for secondary embryonic fields. *Dev. Biol.* **96**, 375–385. (doi:10.1016/0012-1606(83)90175-6)
14. Irvine KD, Rauskolb C. 2001 Boundaries in development: formation and function. *Annu. Rev. Cell Dev. Biol.* **17**, 189–214. (doi:10.1146/annurev.cellbio.17.1.189)
15. Pickett STA, Cadenasso ML. 1995 Landscape ecology: spatial heterogeneity in ecological systems. *Science* **269**, 331–334. (doi:10.1126/science.269.5222.331)
16. Clobert J, Le Galliard J-F, Cote J, Meylan S, Massot M. 2009 Informed dispersal, heterogeneity in animal dispersal syndromes and the dynamics of spatially structured populations. *Ecol. Lett.* **12**, 197–209. (doi:10.1111/j.1461-0248.2008.01267.x)
17. Cobbold CA, Lutscher F, Sherratt JA. 2015 Diffusion-driven instabilities and emerging spatial patterns in patchy landscapes. *Ecol. Complex.* **24**, 69–81. (doi:10.1016/j.ecocom.2015.10.001)
18. Bassett A, Krause AL, Van Gorder RA. 2017 Continuous dispersal in a model of predator–prey–subsidy population dynamics. *Ecol. Modell.* **354**, 115–122. (doi:10.1016/j.ecolmodel.2017.02.017)
19. Kurowski L, Krause AL, Mizuguchi H, Grindrod P, Van Gorder RA. 2017 Two-species migration and clustering in two-dimensional domains. *Bull. Math. Biol.* **79**, 2302–2333. (doi:10.1007/s11538-017-0331-0)
20. Crampin EJ, Hackborn WW, Maini PK. 2002 Pattern formation in reaction–diffusion models with nonuniform domain growth. *Bull. Math. Biol.* **64**, 747–769. (doi:10.1006/bulm.2002.0295)
21. Krause AL, Ellis MA, Van Gorder RA. 2019 Influence of curvature, growth, and anisotropy on the evolution of Turing patterns on growing manifolds. *Bull. Math. Biol.* **81**, 759–799. (doi:10.1007/s11538-018-0535-y)
22. Sun G-Q, Jusup M, Jin Z, Wang Y, Wang Z. 2016 Pattern transitions in spatial epidemics: mechanisms and emergent properties. *Phys. Life Rev.* **19**, 43–73. (doi:10.1016/j.plrev.2016.08.002)
23. Belmonte-Beitia J, Woolley TE, Scott JG, Maini PK, Gaffney EA. 2013 Modelling biological invasions: individual to population scales at interfaces. *J. Theor. Biol.* **334**, 1–12. (doi:10.1016/j.jtbi.2013.05.033)
24. Breña Medina VF, Avitabile D, Champneys AR, Ward MJ. 2015 Stripe to spot transition in a plant root hair initiation model. *SIAM J. Appl. Math.* **75**, 1090. (1119doi:10.1137/140964527)
25. Avitabile D, Breña Medina VF, Ward MJ. 2018 Spot dynamics in a reaction–diffusion model of plant root hair initiation. *SIAM J. Appl. Math.* **78**, 291–319. (doi:10.1137/17M1120932)
26. Benson DL, Sherratt JA, Maini PK. 1993 Diffusion driven instability in an inhomogeneous domain. *Bull. Math. Biol.* **55**, 365–384. (doi:10.1016/S0092-8240(05)80270-8)
27. Page K, Maini PK, Monk NAM. 2003 Pattern formation in spatially heterogeneous Turing reaction–diffusion models. *Physica D* **181**, 80–101. (doi:10.1016/S0167-2789(03)00068-X)
28. Page KM, Maini PK, Monk NAM. 2005 Complex pattern formation in reaction–diffusion systems with spatially varying parameters. *Physica D* **202**, 95–115. (doi:10.1016/j.physd.2005.01.022)
29. Iron D, Ward MJ. 2001 Spike pinning for the Gierer–Meinhardt model. *Math. Comput. Simul.* **55**, 419–431. (doi:10.1016/S0378-4754(00)00303-7)
30. Ward MJ, McInerney D, Houston P, Gavaghan D, Maini P. 2002 The dynamics and pinning of a spike for a reaction–diffusion system. *SIAM J. Appl. Math.* **62**, 1297–1328. (doi:10.1137/S0036139900375112)
31. Wei J, Winter M, Yang W. 2017 Stable spike clusters for the precursor Gierer–Meinhardt system in $\mathbb{R}^2$. *Calculus Var. Partial Differ. Eq.* **56**, 142. (doi:10.1007/s00526-017-1233-6)
32. Krause AL, Klika V, Woolley TE, Gaffney EA. 2018 Heterogeneity induces spatiotemporal oscillations in reaction–diffusion systems. *Phys. Rev. E* **97**, 052206. (doi:10.1103/PhysRevE.97.052206)
33. Kolokolnikov T, Wei J. 2018 Pattern formation in a reaction–diffusion system with space-dependent

feed rate. *SIAM Rev.* **60**, 626–645. (doi:10.1137/17M1116027)

34. Auchmuty JFG, Nicolis G. 1975 Bifurcation analysis of nonlinear reaction–diffusion equations—I. Evolution equations and the steady state solutions. *Bull. Math. Biol.* **37**, 323–365. (doi:10.1016/s0092-8240(75)80036-x)
35. Doelman A, van Heijster P, Shen J. 2018 Pulse dynamics in reaction–diffusion equations with strong spatially localized impurities. *Phil. Trans. R. Soc. A* **376**, 20170183. (doi:10.1098/rsta.2017.0183)
36. Kozák M, Gaffney EA, Klika V. 2019 Pattern formation in reaction-diffusion systems with piecewise kinetic modulation: an example study of heterogeneous kinetics. *Phys. Rev. E* **100**, 042220. (doi:10.1103/PhysRevE.100.042220)
37. Lengyel I, Epstein IR. 1991 Modeling of Turing structures in the chlorite–iodide–malonic acid–starch reaction system. *Science* **251**, 650. (652doi:10.1126/science.251.4994.650)
38. Epstein IR, Showalter K. 1996 Nonlinear chemical dynamics: oscillations, patterns, and chaos. *J. Phys. Chem.* **100**, 13132–13147. (doi:10.1021/jp953547m)
39. Rüdiger S, Míguez DG, Munuzuri AP, Sagués F, Casademunt J. 2003 Dynamics of Turing patterns under spatiotemporal forcing. *Phys. Rev. Lett.* **90**, 128301. (doi:10.1103/PhysRevLett.90.128301)
40. Míguez DG, Pérez-Villar V, Muñuzuri AP. 2005 Turing instability controlled by spatiotemporal imposed dynamics. *Phys. Rev. E* **71**, 066217. (doi:10.1103/PhysRevE.71.066217)
41. Rüdiger S, Nicola EM, Casademunt J, Kramer L. 2007 Theory of pattern forming systems under traveling-wave forcing. *Phys. Rep.* **447**, 73–111. (doi:10.1016/j.physrep.2007.02.017)
42. Yang L, Dolnik M, Zhabotinsky AM, Epstein IR. 2002 Spatial resonances and superposition patterns in a reaction–diffusion model with interacting Turing modes. *Phys. Rev. Lett.* **88**, 208303. (doi:10.1103/PhysRevLett.88.208303)
43. Peter R, Hilt M, Ziebert F, Bammert J, Erlenkämper C, Lorscheid N, Weitenberg C, Winter A, Hammele M, Zimmermann W. 2005 Stripe–hexagon competition in forced pattern-forming systems with broken up-down symmetry. *Phys. Rev. E* **71**, 046212. (doi:10.1103/PhysRevE.71.046212)
44. Haim L, Hagberg A, Meron E. 2015 Non-monotonic resonance in a spatially forced Lengyel-Epstein model. *Chaos* **25**, 064307. (doi:10.1063/1.4921768)
45. Dewel G, Borckmans P. 1989 Effects of slow spatial variations on dissipative structures. *Phys. Lett. A* **138**, 189–192. (doi:10.1016/0375-9601(89)90025-X)
46. Kuske R, Eckhaus W. 1997 Pattern formation in systems with slowly varying geometry. *SIAM J. Appl. Math.* **57**, 112–152. (doi:10.1137/S0036139994277531)
47. Otsuji M, Ishihara S, Co C, Kaibuchi K, Mochizuki A, Kuroda S. 2007 A mass conserved reaction–diffusion system captures properties of cell polarity. *PLoS Comput. Biol.* **3**, e108. (doi:10.1371/journal.pcbi.0030108)
48. Mendez V, Fedotov S, Horsthemke W. 2010 *Reaction-transport systems: mesoscopic foundations, fronts, and spatial instabilities*. New York, NY: Springer-Verlag.
49. Klika V, Kozák M, Gaffney EA. 2018 Domain size driven instability: self-organization in systems with advection. *SIAM J. Appl. Math.* **78**, 2298–2322. (doi:10.1137/17M1138571)
50. Klika V. 2017 Significance of non-normality-induced patterns: Transient growth versus asymptotic stability. *Chaos* **27**, 073120. (doi:10.1063/1.4985256)
51. Maini PK, Woolley TE, Baker RE, Gaffney EA, Lee SS. 2012 Turing's model for biological pattern formation and the robustness problem. *Interface Focus* **2**, 487–496. (doi:10.1098/rsfs.2011.0113)
52. Woolley TE, Baker RE, Maini PK. 2017 In *The incomputable*, pp. 219–235. Berlin, Germany: Springer.
53. Dwyer HI, Zettl A. 1995 Electronic Journal of Differential Equations (EJDE)[electronic only] **1995**.
54. Malamud MM. 2005 In *Sturm-Liouville Theory*, pp. 237–270. Berlin, Germany: Springer.
55. Bremmer H. 1951 The W.K.B. approximation as the first term of a geometric-optical series. *Commun. Pure Appl. Math.* **4**, 105–115. (doi:10.1002/cpa.3160040111)
56. Alder K, Pauli HKA. 1969 Quantal corrections and the WKB approximation of multiple Coulomb excitation. *Nucl. Phys. A* **128**, 193–208. (doi:10.1016/0375-9474(69)90985-3)
57. Griffiths DJ, Schroeter DF. 2018 *Introduction to quantum mechanics*. Cambridge, UK: Cambridge University Press.
58. Bender CM, Orszag SA. 2013 *Advanced mathematical methods for scientists and engineers I: asymptotic methods and perturbation theory*. Springer Science & Business Media.
59. Tennyson CN, Klamut HJ, Worton RG. 1995 The human dystrophin gene requires 16 hours to be transcribed and is cotranscriptionally spliced. *Nat. Genet.* **9**, 184–190. (doi:10.1038/ng0295-184)
60. Singh J, Padgett RA. 2009 Rates of *in situ* transcription and splicing in large human genes. *Nat. Struct. Mol. Biol.* **16**, 1128–1133. (doi:10.1038/nsmb.1666)
61. Sekine R, Shibata T, Ebisuya M. 2018 Synthetic mammalian pattern formation driven by differential diffusivity of Nodal and Lefty. *Nat. Commun.* **9**, 5456. (doi:10.1038/s41467-018-07847-x)
62. Crawford JD. 1991 Introduction to bifurcation theory. *Rev. Mod. Phys.* **63**, 991. (1037doi:10.1103/RevModPhys.63.991)
63. Wollkind DJ, Manoranjan VS, Zhang L. 1994 Weakly nonlinear stability analyses of prototype reaction–diffusion model equations. *SIAM Rev.* **36**, 176–214. (doi:10.1137/1036052)
64. Stephenson LE, Wollkind DJ. 1995 Weakly nonlinear stability analyses of one-dimensional Turing pattern formation in activator–inhibitor/immobilizer model systems. *J. Math. Biol.* **33**, 771–815. (doi:10.1007/BF00187282)
65. Chen Y, Buceta J. 2019 A non-linear analysis of Turing pattern formation. *PLoS ONE* **14**, e0220994. (doi:10.1371/journal.pone.0220994)
66. Gierer A, Meinhardt H. 1972 A theory of biological pattern formation. *Kybernetik* **12**, 30–39. (doi:10.1007/BF00289234)
67. Turing AM. 1950 I.–Computing machinery and intelligence. *Mind* **59**, 433–460. (doi:10.1093/mind/LIX.236.433)